frontiers

Information processing and learning within an in vitro epilepsy-like model expressing glutamatergic hyperactivity following pharmacological intervention

Bradley Watmuff[1*], Forough Habibollahi[1], Candice Desouza[1], Moein Khajehnejad[2], Alon Loeffler[1], Koby Baranes[3, 4], Noah Poulin[3, 4], Mark Kotter[3, 4, 5], Brett J. Kagan[1, 6]

[1]Cortical Labs, Australia, [2]Turner Institute for Brain and Mental Health, Monash University, Australia, [3]Department of Clinical Neuroscience, School of Clinical Medicine, University of Cambridge, United Kingdom, [4]Wellcome Trust - Medical Research Council Cambridge Stem Cell Institute, School of Biological Sciences, University of Cambridge, United Kingdom, [5]Bit Bio LTD., United Kingdom, [6]Department of Biochemistry and Pharmacology, School of Biomedical Sciences, Faculty of Medicine, Dentistry and Health Sciences, University of Melbourne, Australia

In review

Submitted to Journal:
Frontiers in Cellular Neuroscience

Specialty Section:
Cellular Neurophysiology

Article type:
Original Research Article

Manuscript ID:
1375611

Received on:
24 Jan 2024

Journal website link:
www.frontiersin.org

Scope Statement

This work furthers our understanding of the pharmacological effects of anti-seizure drugs on human iPSC-derived inducible NGN2 glutamatergic neurons. It shows that these compounds both reduce neuronal culture activity and, when embedded in the DishBrain information processing platform, improve measures of gameplay in a dose-dependent manner. We also examine more subtle parameters from electrophysiological data such as neural criticality and functional connectivity and find distinct differences between control and treated groups as well as between rest and active gameplay. Our study falls directly under the guise of novel Cellular Neurophysiology, and is intended to form part of a current Research Topic in this journal, highlighting the relevance of the study for this Journal's scope.

Conflict of interest statement

The authors declare a potential conflict of interest and state it below

BW, FH, CD, MK, AL, and BJK are employed by CCLABS Pty Ltd, a for-profit company with an interest in the commercial viability of synthetic biological intelligence.

The author(s) declared that they were an editorial board member of Frontiers, at the time of submission. This had no impact on the peer review process and the final decision

In review

CRediT Author Statement

Alon Loeffler: Writing – original draft, Writing – review & editing. Bradley Watmuff: Writing – original draft, Writing – review & editing. Brett J. Kagan: Writing – original draft, Writing – review & editing. Candice Desouza: Writing – original draft, Writing – review & editing. Forough Habibollahi: Writing – original draft, Writing – review & editing. Koby Baranes: Writing – review & editing. Mark Kotter: Writing – review & editing. Moein Khajehnejad: Writing – original draft, Writing – review & editing. Noah Poulin: Writing – review & editing.

Keywords

IPSC, MEA, Electrophysiology, disease model, Neuroscience, Epilepsy, Drug Discovery

Abstract

Word count: 324

The brain's function mainly consists in the computation of information. In contrast, cellular and molecular neuroscience research focusses on measurements of cellular states. For a preclinical assay to predict the pharmacological efficacy of a compound it must model physiological states. By using DishBrain, an in vitro assay capable of embodying neural cultures in a simulated game-world, it is possible to quantify the information-processing capacity of in vitro neural cultures and determine drug dose-response profiles. Glutamatergic neuron hyperactivity is associated with numerous psychiatric and neurological conditions. Excess glutamate is particularly associated with generating and propagating epileptic seizures, and drugs which control epilepsy often reduce glutamatergic neurotransmission. Here, the inducible overexpression of neurogenin 2 (NGN2) in human induced pluripotent stem cells (hiPSCs) was used to generate near-pure glutamatergic neural cultures. Conventional anti-seizure drugs (ASDs) were trialed to determine their effects on the activity of this in vitro model when embodied in the game-world through closed-loop real-time electrophysiological stimulation and recordings. Spontaneous activity and gameplay sessions were recorded from multielectrode arrays (MEA) daily from day 21 of differentiation. Cultures were then treated with either DMSO vehicle control, Phenytoin 10-33 µM, Perampanel 1-10 µM, or Carbamazepine 2-200 µM. MEA recordings revealed electrophysiological activity increased significantly over days as cultures developed. Carbamazepine 200 µM reduced maximum firing rate significantly compared to time-matched vehicle control, at the same time as increasing key measures of gameplay performance (hit/miss ratio and mean rally length) from the start of gameplay compared to the end. This is the first time that altered performance in an in vitro model of synthetic biological intelligence (SBI) by therapeutic compounds has been demonstrated. Interestingly, only dishes treated with functionally inhibitory compounds exhibited measurable goal-directable activity changes, suggesting a link between the attenuation of glutamatergic hyperactivity and gameplay performance. Neurocomputational analysis of detailed electrophysiological dynamics of these cultures further revealed nuances in the activity responses to closed-loop stimulation with different pharmacological interventions not observable through examining only spontaneous activity.

Funding information

CCLABS Pty Ltd. provided all funding for the equipment and reagents necessary for the completion of this work, except where otherwise noted in the text.

Funding statement

The author(s) declare financial support was received for the research, authorship, and/or publication of this article.

Ethics statements

Studies involving animal subjects
Generated Statement: No animal studies are presented in this manuscript.

Studies involving human subjects
Generated Statement: Ethical approval was not required for the studies involving humans because Human cell lines were generated in a previous study.. The studies were conducted in accordance with the local legislation and institutional requirements. The human samples used in this study were acquired from gifted from another research group. Written informed consent to participate in this study was not required from the participants or the participants' legal guardians/next of kin in accordance with the national legislation and the institutional requirements.

Inclusion of identifiable human data
Generated Statement: No potentially identifiable images or data are presented in this study.

Data availability statement

Generated Statement: The datasets presented in this study can be found in online repositories. The names of the repository/repositories and accession number(s) can be found in the article/supplementary material.

In review

Information processing and learning within an *in vitro* epilepsy-like model expressing glutamatergic hyperactivity following pharmacological intervention.

Bradley Watmuff[1], Forough Habibollahi[1], Candice Desouza[1], Moein Khajehnejad[2], Alon Loeffler[1], Koby Baranes[3,4], Noah Poulin[3,4], Mark Kotter[3,4,5] and Brett J. Kagan*[1, 6]

[1] Cortical Labs Pty. Ltd., Melbourne, VIC, Australia

[2]Turner Institute for Brain and Mental Health, Monash University, Clayton, 3800, VIC, Australia.

[3] Department of Clinical Neurosciences, University of Cambridge, Cambridge CB2 0QQ, United Kingdom

[4] Wellcome-MRC Cambridge Stem Cell Institute, University of Cambridge, Cambridge CB2 0AW, United Kingdom

[5] Bit Bio LTD, Cambridge, United Kingdom

[6] Department of Biochemistry and Pharmacology, University of Melbourne, Parkville, VIC, Australia.

* Corresponding Author:

brett@corticallabs.com

Keywords: iPSC, MEA, electrophysiology, disease model, neuroscience, epilepsy, drug discovery. (Min.5-Max. 8)

In review

Abstract

The brain's function mainly consists in the computation of information. In contrast, cellular and molecular neuroscience research focusses on measurements of cellular states. For a preclinical assay to predict the pharmacological efficacy of a compound it must model physiological states. By using *DishBrain*, an *in vitro* assay capable of embodying neural cultures in a simulated game-world, it is possible to quantify the information-processing capacity of *in vitro* neural cultures and determine drug dose-response profiles. Glutamatergic neuron hyperactivity is associated with numerous psychiatric and neurological conditions. Excess glutamate is particularly associated with generating and propagating epileptic seizures, and drugs which control epilepsy often reduce glutamatergic neurotransmission. Here, the inducible overexpression of neurogenin 2 (NGN2) in human induced pluripotent stem cells (hiPSCs) was used to generate near-pure glutamatergic neural cultures. Conventional anti-seizure drugs (ASDs) were trialed to determine their effects on the activity of this *in vitro* model when embodied in the game-world through closed-loop real-time electrophysiological stimulation and recordings. Spontaneous activity and gameplay sessions were recorded from multielectrode arrays (MEA) daily from day 21 of differentiation. Cultures were then treated with either DMSO vehicle control, Phenytoin 10-33 µM, Perampanel 1-10 µM, or Carbamazepine 2-200 µM. MEA recordings revealed electrophysiological activity increased significantly over days as cultures developed. Carbamazepine 200 µM reduced maximum firing rate

significantly compared to time-matched vehicle control, at the same time as increasing key measures of gameplay performance (hit/miss ratio and mean rally length) from the start of gameplay compared to the end. This is the first time that altered performance in an *in vitro* model of synthetic biological intelligence (SBI) by therapeutic compounds has been demonstrated. Interestingly, only dishes treated with functionally inhibitory compounds exhibited measurable goal-directable activity changes, suggesting a link between the attenuation of glutamatergic hyperactivity and gameplay performance. Neurocomputational analysis of detailed electrophysiological dynamics of these cultures further revealed nuances in the activity responses to closed-loop stimulation with different pharmacological interventions not observable through examining only spontaneous activity.

Introduction

Predicting the clinical efficacy of a pharmacological intervention targeting a disease *in vitro* requires viable assays that physiologically capture the key processes and functions of the tissue or organ it proposes to model. It is likely that no other biological system is as challenging to meaningfully model as neural systems. Neurons are highly dynamic cell types whose primary function is to send, receive and transform electrical signals throughout the brain and periphery. Current *in vitro* models typically provide no stimulation to neural cells, with even state-of-the-art approaches using spontaneous activity or basic evoked activity as a functional outcome (Campos et al., 2018). Yet, neural systems do not merely fire action potentials, but process structured information and alter their own activity in meaningful ways. To do this effectively, neural systems must be able to modulate their activity in response to a variety of cellular and environmental inputs (Shahaf and Marom, 2001; Mileva et al., 2008; Ly et al., 2012; Ghaderi et al., 2018). The use of a Synthetic Biological Intelligence (SBI) assay, as recently described (Kagan et al., 2023), may provide the opportunity to assess not only the functional properties of a disease model, but also nuances that arise in response to pharmacological intervention. By creating a structured information landscape through a real-time closed-loop patterning of electrophysiological stimulation and recording, *in vitro* neural cultures can be embodied within a simulated game-world environment, in this case representing a simplified version of the game *Pong*. The observation of learning effects has also been replicated in other environments with various inputs and supports the idea that exploring the information processing capacity of *in vitro* neurons offers a compelling pathway forward (Cai et al., 2023). Previous work also demonstrated that cultures of cortical neurons within the *DishBrain* system displayed activity changes consistent with goal-directed learning, with significant increases in gameplay performance over time (Kagan et al., 2022b). Moreover, these networks displayed population network activity metrics such as close to critical dynamics (Habibollahi et al., 2023). However, prior work has focused on *in vitro* neural cultures intended to model phenotypically 'healthy' neural activity. Exploring the behaviour of neural cell cultures

In review

designed to model disease characteristics would determine the viability of using SBI systems to test disease models and screen pharmacological interventions.

Glutamatergic hyperactivity dysregulation is a state where excitatory forebrain neurons' activity is high frequency, continuous and non-synchronised (Miladinovic et al., 2015). Post-mortem studies have associated irregular glutamate signalling with a number of neurological and psychiatric conditions (Miladinovic et al., 2015). A disease commonly associated with glutamatergic hyperactivity is epilepsy (Galanopoulou et al., 2012; Nieto-Estévez and Hsieh, 2020; Negraes et al., 2021). Despite several available disease-modifying therapies, approximately 30% of patients with epilepsy do not respond to these treatments (Kwan et al., 2011). As with many other neurological diseases, pre-clinical research to develop new ASDs has predominantly leveraged rodent models (Putnam and Merritt, 1937; Golyala and Kwan, 2017). The limitations of such models are well recognized and translate into poor clinical trial outcomes (Galanopoulou et al., 2012). It is likely that the pathophysiology of human drug-resistant epilepsy, with recurrent spontaneous seizures, is not adequately recapitulated in induced-seizure rodent models. For this reason, in vitro epileptic-like cellular models have been developed (Nieto-Estévez and Hsieh, 2020). The ability to demonstrate compelling dose-response curves in these *in vitro* models would be highly useful for drug discovery. Moreover, this could enable a personalized medicine approach: culturing cells from patients which display drug-resistant phenotypes, while reducing the need for animal testing (Kagan et al., 2022a, 2023).

In review

Previous work has leveraged neurogenin 2 (NGN2)-reprogrammed neurons to create an *in vitro* model of epilepsy (Alaverdian et al., 2023). By utilizing a robust forward programming platform for Optimized inducible Overexpression (OPTi-OX) of NGN2, human induced pluripotent stem cells (hiPSC) can reproducibly generate neuronal populations with glutamatergic hyperexcitability (Ho et al., 2016; Pawlowski et al., 2017). Here we aimed to use these neuronal cultures as a simple *in vitro* epilepsy model with a focus on hyperexcitability. By assessing the electrophysiological development of these cultures over time, we evaluated the suitability of validity of the *DishBrain* system for disease modelling and drug screening. Finally, given the role of neurocomputational metrics such as neural criticality in predicting phenotypically normal behaviours in vivo, and the link these metrics have to epilepsy, we also assessed the population dynamics of these cultures during spontaneous activity and during gameplay in the *DishBrain* system (Arviv et al., 2016; Zimmern, 2020; Habibollahi et al., 2023).

Specifically, we hypothesized that NGN2-reprogrammed iNeuron cultures would demonstrate increased gameplay performance and phenotypically normalized electrophysiological population dynamics following the administration of existing anti-seizure drugs.

Materials and Methods

IPSC Culture

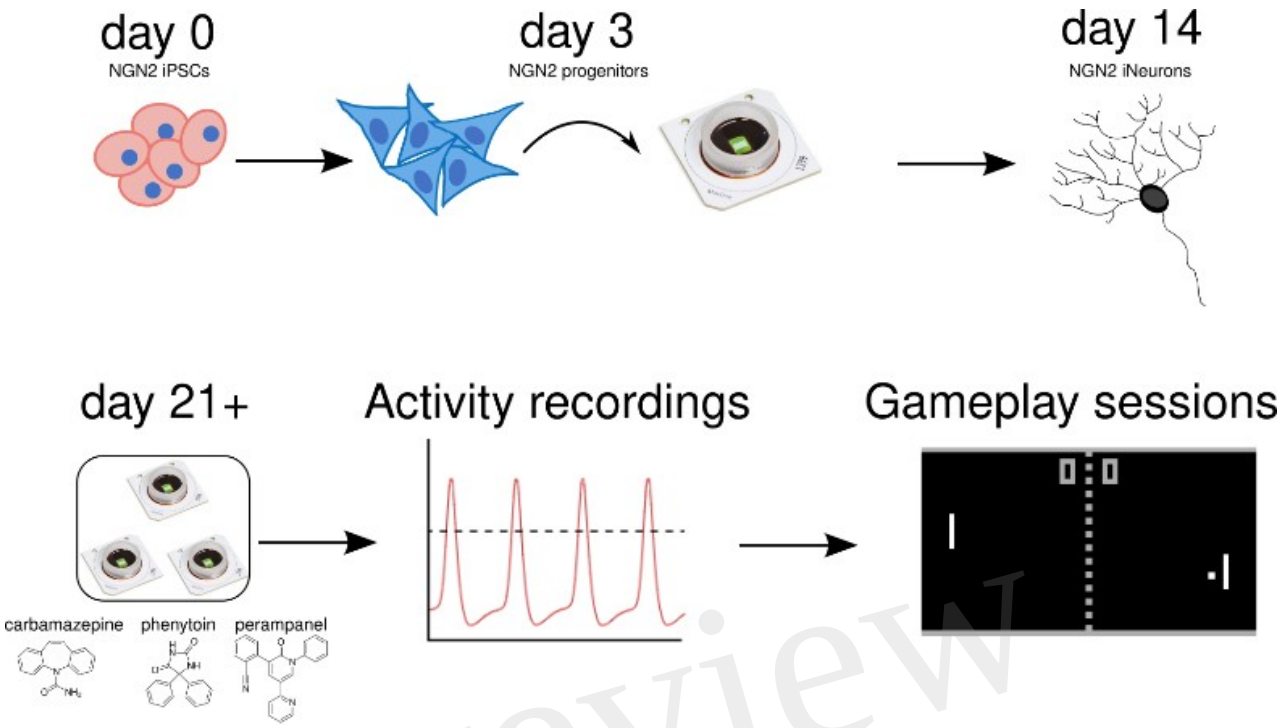

Figure 1: Overview of study design.

A broad overview of the study methodology including cell culture can be seen in Figure 1. All cultures were maintained in a 37°C, 5% CO2, 5% O2 humidified cell culture incubator (BINDER, Germany). NGN2 iPSCs were thawed on vitronectin (VTN, ThermoFisher, Australia)-coated T25 flasks (18 µL VTN to 1.8 mL DPBS containing Ca^{2+}/Mg^{2+}, washed with 4 mL DPBS prior to cell seeding) and maintained in 4 mL StemFlex iPSC media (ThermoFisher, Australia). Cells were passaged using EDTA (0.5 mM in DPBS).

Neuronal Differentiation

To initiate differentiation, NGN2 iPSCs (Pawlowski et al., 2017) were dissociated with Accutase (Sigma Aldrich, Australia) and seeded on Geltrex (ThermoFisher, Australia)-coated 24 well plates at a concentration of 80000 cell per cm2 in 1 mL StemFlex media with 5 µM Y-27632. The next day (day 0), cells were washed with 1 mL DPBS and media changed to Day 0-1 media (Table 1) containing doxycycline 2 µg / mL (DOX, Sigma Aldrich, Australia). Cells were maintained in this media until day 2, when cells were washed with 1 mL DPBS and media changed to Day ≥ 2 media (Table 1) containing DOX 2 µg / mL. On day 3, cells were washed with DPBS, dissociated with Accutase and plated on to Poly-D-Lysine-Geltrex coated MaxONE multi electrode array chips (Maxwell BioSystems, Switzerland) in Day ≥ 2 media (Table 1) containing DOX (2 µg /mL) and 5 uM Y-27632. 200000 NGN2 cells, and 50000 primary human cortical astrocytes (Sciencell Cat# 1800, USA; maintained previously according to manufacturer's specifications) were mixed and plated on

In review

each MEA chip at this time. On days 4 and 5, full media changes in Day ≥ 2 media + DOX were performed. On day 7, media was changed to Day ≥ 2 media without DOX. Thereafter, half media changes were performed every second day.

Table 1: Cell culture media used in neural differentiation in the present study.

Formula	Item	Amount
Day 0-1 media	DMEM/F12 (31330-038, Fisher Scientific)	50 mL
	P/S (11548876, Fisher Scientific)	500 µl
	NEAA (11-140-050, Fisher Scientific)	500 µl
	Glutamax (35050038, ThermoFisher)	500 µl
	2-ME (31350010, ThermoFisher)	50 µl
	N2 supplement (17502-048, ThermoFisher)	500 µL
	Doxycycline (2mg/mL)	50 uL (2 µg/mL)
Day 2 onwards (D ≥ 2) media	Neurobasal (21103049, ThermoFisher)	50 mL
	P/S (11548876, Fisher Scientific)	500 µl
	Glutamax (35050038, ThermoFisher)	500 µl
	2-ME (31350010, ThermoFisher)	50 µl
	B27 supplement (17504044, ThermoFisher)	1 mL
	BDNF (50 µg/mL)	10 µl (10 ng/ml)
	NT3 (50 µg/mL)	10 µl (10 ng/ml)
	Doxycycline (2 mg/mL)	50 µL (2 ug/mL)

In review

Immunocytochemistry

From day 35 onwards, cultures grown in parallel on plastic tissue culture treated 24-well plates were washed free of media (3 × 5 min in DPBS -/-) and fixed in 4% paraformaldehyde aqueous solution (Electron Microscopy Services, USA) for 15 min at RT. Wells were washed once with DPBS and then permeabilized with 0.1% Triton X-100 (Sigma-Aldrich, Australia) in PBS for 30 min at RT. Cells were then blocked with 1% normal goat serum in PBS for 30 min and incubated overnight at 4°C in 0.1% Triton X-100 in DPBS with the primary antibodies shown in Table 2. The next day, after another 3 washes, secondary antibodies as shown in Table 2 were incubated with the cells for 2 h at room temperature. Cells were again washed 3 times and DAPI (ThermoFisher, Australia) was briefly added for 5 min prior to visualisation. Cells were visualised using a Nikon A1Plus Ti ZDrive confocal microscope (Nikon, Japan), and at least three images (2048 x 2048 pixels with 161 z-steps of 0.7 µm) were recorded per well.

Table 2: Antibodies used in immunocytochemistry experiments.

Group	Antibody	Usage
Primary	Anti-VGLUT2 (Abcam USA, ab79157)	1:1000
	Anti-FOXG1 (Abcam USA, ab196868)	1:100
	Anti-MAP2 (Abcam USA, ab5392)	1:5000
	Anti-PSD-95 (Abcam USA, ab192797)	1:1000
	Anti-SYN1 (Abcam USA, ab254349)	1:500
	Anti-GFAP (Abcam USA, ab4674)	1:500

	Anti-TUJ1 (Merck Australia, MAB1637)	1:1000
Secondary	Gt anti rabbit 488 (Abcam USA, ab150077)	1:1000
	Gt anti chicken 555 (Abcam USA, ab159170)	1:1000
	Gt anti mouse 647 (Sigma Aldrich Australia, SAB4600183)	1:1000
Stain	DAPI 1 mg / mL (ThermoFisher Australia, 62248)	1:10000

Single Cell RNA Sequencing

Human iPSCs (D0) and iNeurons (D7, D14, D21) were washed once with 1X dPBS before adding either Accutase (D0) or Accutase containing 20 units/mL of papain, 5mM MgCl2 and 5mg/mL DNase I (Worthington, United Kingdom) (D7-D21). The cells were incubated at 37°C for up to 5 min (D0) or up to 45 min (D7-D21) before adding DMEM:F12 (ThermoFisher, United Kingdom) supplemented with 10% FBS (Sigma). The cells were dissociated using a P1000 and collected in a 15mL tube. After centrifugation, the cells were resuspended in 1X dPBS containing 1% BSA (Sigma) and 10µM Rock inhibitor (Tocris, United Kingdom) and collected in a 15mL tube capped with a 40µm cell strainer. Following centrifugation, cells were washed 3 additional times. Single-cell suspensions were counted using an automated cell counter (Countess, Invitrogen, United Kingdom) and concentrations adjusted to 1000 cells/mL. Cells were then hash-tagged using total-seq anti-human hashtag antibody (BioLegend, United Kingdom) and kept on ice for further processing.

Single cell suspensions were processed by the Chromium Controller using Chromium Single Cell 3' Reagent Kit v2 by 10x Genomics. Each sample was loaded for a target recovery of 8000 cells per sample. All the steps were performed according to the manufacturer's specifications. All samples were sequenced using the Illumina HiSeq platform, with 50,000 reads on average per cell. scRNAseq samples were processed using the 10x Genomics CellRanger pipeline v3.0.1 using the GRCh38 genome assembly to produce the gene expression matrices. The filtered gene expression matrix was used without modifying any cell gating parameters.

Standard quality control was performed in R (v.4.3.1) using Seurat (v.4.4.0): Cells with mitochondrial RNA below 5% and with 200 to 10000 genes were included. Counts were scaled and mean expression levels at each timepoint were normalized to day 0 (hiPSCs) for visualization.

Electrophysiology and *DishBrain* Pharmacology

MEA chip activity was assessed by performing activity recordings using MaxWell MaxONE software at regular timepoints during neuronal differentiation. Briefly, MEA chips were removed from the cell culture incubator and placed on MaxWell readers in a non-humidified 37°C 5% CO2 incubator and equilibrated for 10 min before 5 min of full recording. When chips obtained a culture-wide average activity of 0.7 Hz (generally between day 21 and day 35 of differentiation), chips were considered ready for *DishBrain* gameplay. On days where gameplay was performed, cells were removed from the cell culture incubator and an activity assay conducted as above to ensure minimum required activity for gameplay was present. If the chip passed, cells were treated with

In review

one of the following compounds: Phenytoin 10-33 µM, Perampanel 1-10 µM, Carbamazepine 2-200 µM, or DMSO vehicle control, before being returned to the cell culture incubator. After 1 h, cells were returned to the reader for another activity assay, then closed-loop feedback gameplay was started as follows: Rest session (15 min), Active session (15 min), Rest session (15 min), Active session (15 min). After 60 minutes, chips had a full media change (1 mL) and were returned to the cell culture incubator. In Rest sessions, cell responses were recorded and contributed to gameplay, but cells were not stimulated with information encoding the gameplay world. In Active sessions, this information was also provided to the cells. Chips were exposed to 60 min gameplay conditions a maximum of one time per day, and played for up to four consecutive days.

Data Analysis

Activity assay recordings were analysed to measure average spike firing rate and average spike amplitude. From gameplay experiments, hit/miss ratio and rally length were calculated and results summarised for each treatment (drug/dose) group. Summary data is presented as the mean hit/miss ratio or rally length, the standard error of the mean (SEM), and the count (n) of the treatment observations. Significance testing was performed to determine differences, if any, between treatment groups (Student's t-test or one-way ANOVA with post-hoc Bonferroni multiple comparison test compared to DMSO vehicle control). A p value less than 0.05 was taken as the minimum level of significance. The majority of data analysis was performed in Python as described in section results. Initial electrophysiological analyses were performed using the RStudio (Posit Software, PBC) Build 463 IDE with R version 4.3.1 and the following packages: tidyverse version 2.0.0, ggsignif version 0.6.4.

In review

Results

NGN2 iNeuron cultures display glutamatergic and neuronal markers

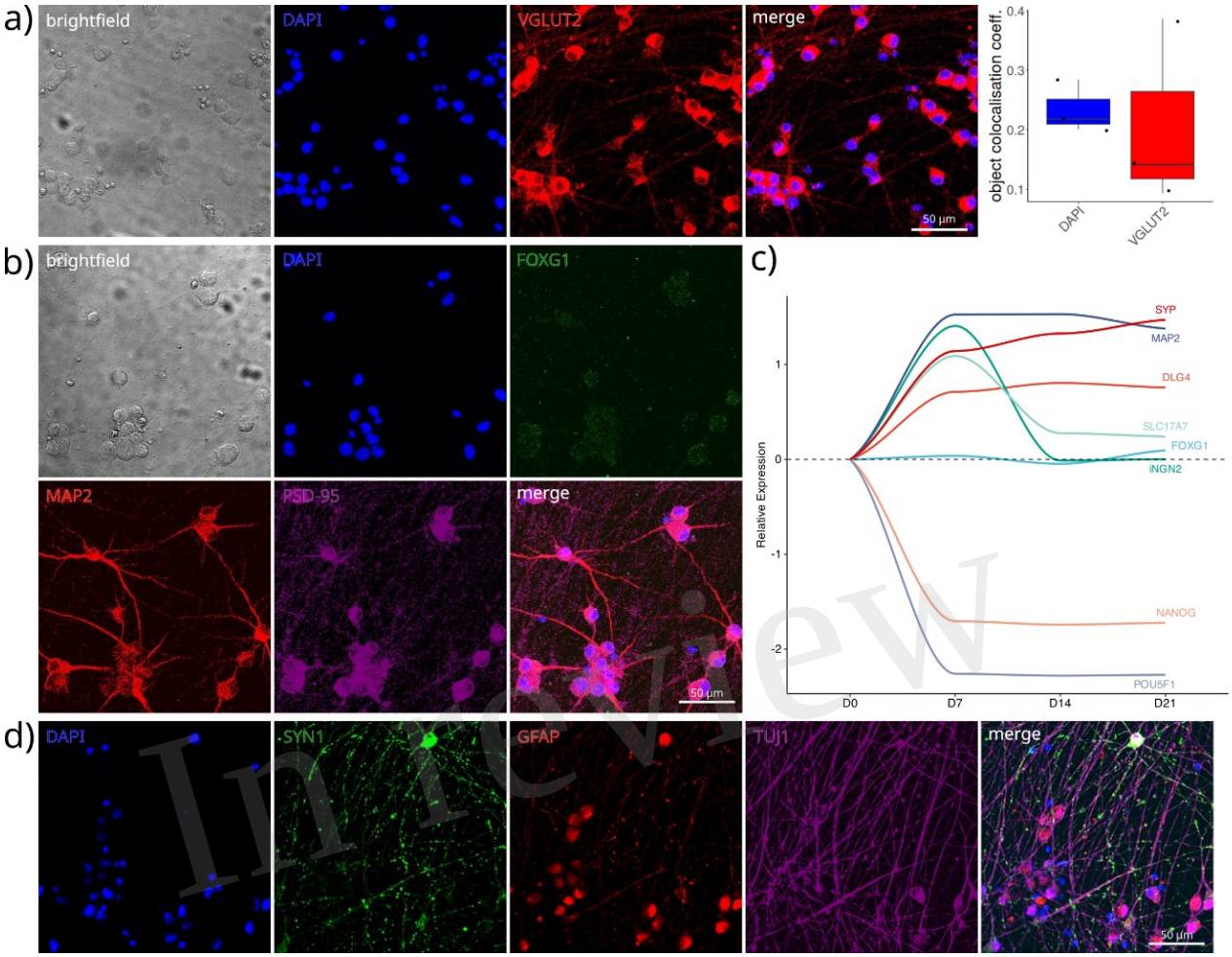

Figure 2: NGN2 cultures express glutamatergic neuron markers. a) Immunocytochemistry of NGN2 cultures at day 38 showing brightfield, DAPI (blue), and VGLUT2 (SLC17A6; red) labelling. Fraction colocalisation of the indicated label with objects of the other label are shown to the right. Scale bar, 50 µm. b) Immunocytochemistry in NGN2 cultures showing brightfield, DAPI (blue), FOXG1 (green), MAP2 (red), and PSD-95 (DLG4; magenta), as well as a merged image. Scale bar, 50 µm. c) Fold changes in expression of neural and cortical transcripts before and during induced differentiation. Mean expression is normalised to day 0 (hiPSCs).

To confirm the glutamatergic nature of the OPTi-OX NGN2 iNeurons, we began by examining common neuronal markers at the transcriptional and protein-levels. Immunocytochemistry of cultures on day 38 revealed the presence of the neuronal markers MAP2 and TUJ1, the synaptic proteins SYN1 and PSD-95, as well as a high level of expression of VGLUT2 (SLC17A6), a marker of glutamatergic neurons (Figure 2, a, b, d). We also confirmed the presence of GFAP, the glial fibrillary protein present in astrocytes (Figure 2, d). We did not observe robust immunolabelling from FOXG1, a transcription factor required for ventral telencephalic development. Single cell RNA-Seq experiments further confirmed the upregulation of neuronal, synaptic, and glutamatergic genes, as well as the downregulation of pluripotency genes, from day 0 to day 21 of differentiation.

In review

SLC17A7 (VGLUT1) and NGN2 expression peaked at day 7 before returning to baseline, and FOXG1 expression did not appear to change during the timepoints measured (Figure 2, c).

NGN2 iNeuron cultures display electrophysiological hyperactivity and pharmacological interventions showcase compound-specific responses

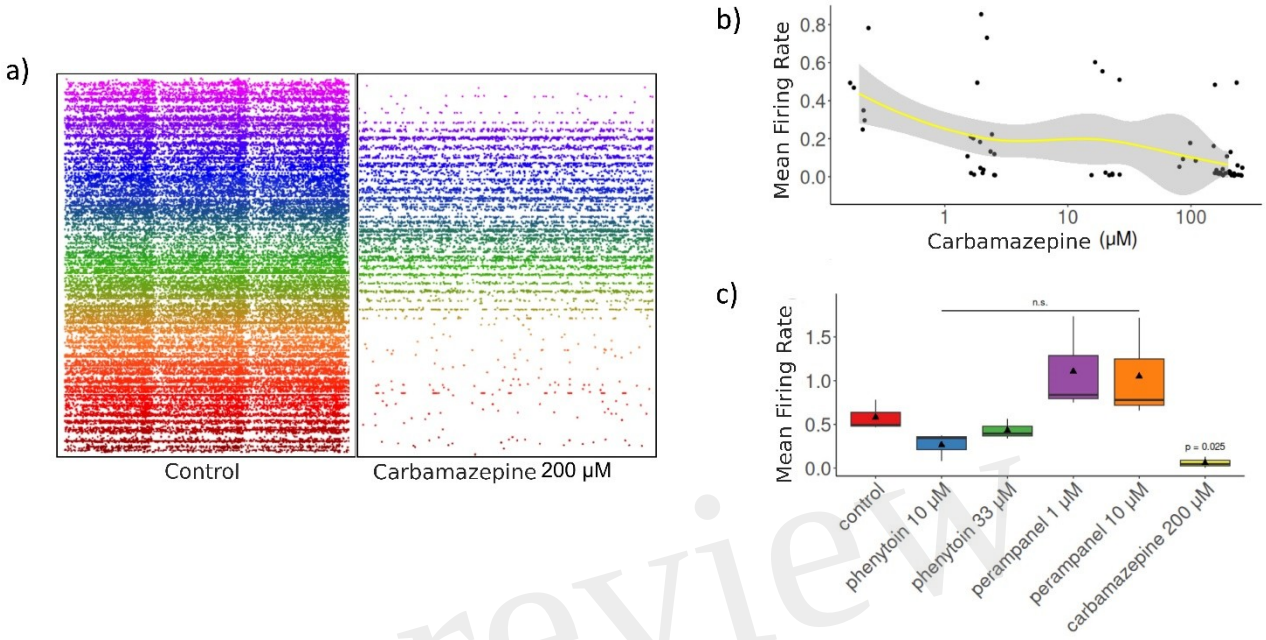

In review

Figure 3: Initial activity testing and pharmacological manipulations. a) Raster plot showing culture firing activity prior to and after Carbamazepine (200 µM) administration at day 28. Each row represents one electrode (of 1024). b) Relationship between mean firing rates and escalating doses of Carbamazepine. Firing rates were calculated per 100 msec for this analysis. c) Analysis of mean firing rate with administration of different pharmacological compounds. Each group was analysed by one-way ANOVA with post-hoc Bonferroni test compared to control.

Having confirmed the glutamatergic identity of the neurons in culture, we turned our attention to characterising their basic functional properties. Cultures developed rapidly over the course of two weeks, from day 7 to day 21, and displayed robust burst and network activity in all channels (Figure 3, a, shows control activity recorded at day 28). We then measured their activity after the application of Carbamazepine, Phenytoin, and Perampanel. Carbamazepine had a marked effect on reducing mean firing rate after 1 h treatment (Figure 3, a), and we observed a dose-response relationship between increasing Carbamazepine dose and reduced mean firing rate (Figure 3, b). At 200 µM, the reduction in firing activity brought about by Carbamazepine treatment was significant (Figure 3, c; $p < 0.05$), however Phenytoin and Perampanel did not significantly affect the firing rate of cultures at either dose tested.

We next investigated the electrophysiological activity of NGN2 cultures during gameplay, and analysed the mean firing rate calculated per second, the variance of the extracted firing rates, and the interspike intervals (ISI). The distribution of these metrics is depicted in Figure 4 (a, d, g), showcasing comparisons between gameplay and rest conditions under control, as well as across

various pharmacological interventions. Statistical comparisons are shown in Figure 4 (b, e, h). Additionally, we explored the same electrophysiological metrics across different doses and compared these to the control group as seen in Figure 4 (c, f, i).

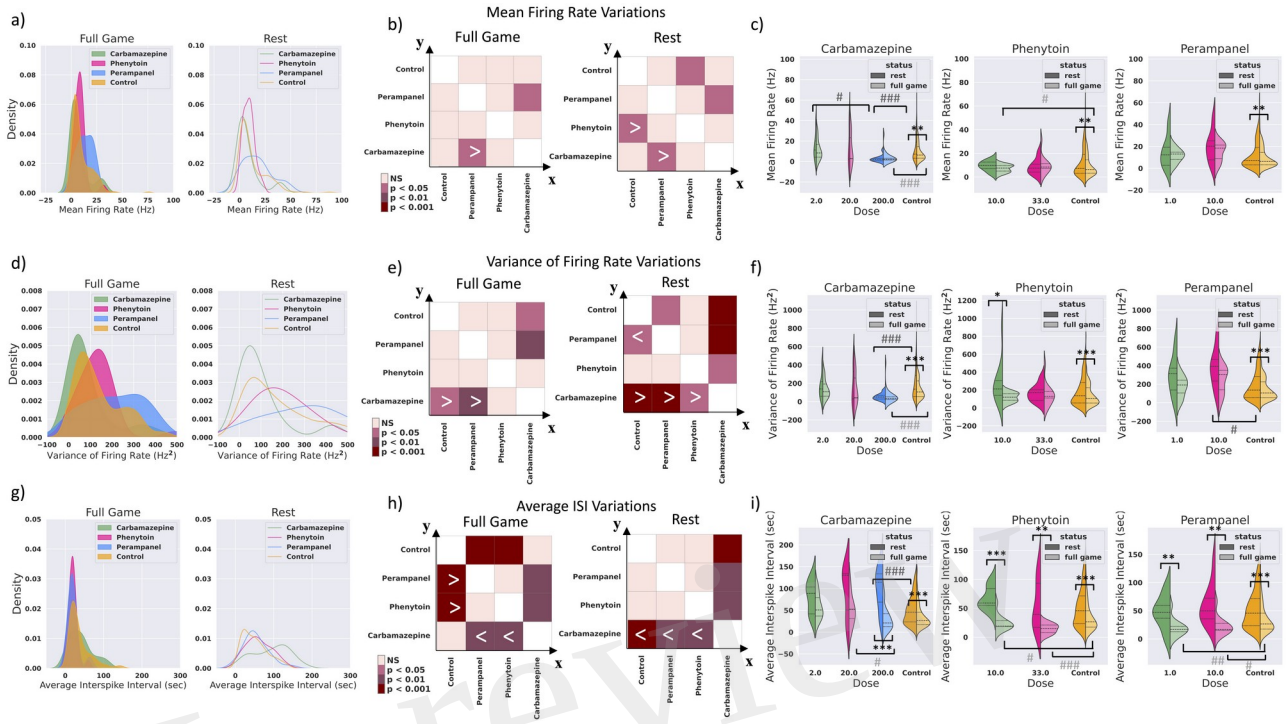

*Figure 4: Firing Statistics under control and pharmacological intervention conditions. a, d, g) Comparison of Mean Firing Rate, Variance of Firing Rate, and Average Interspike Interval (ISI) in both rest and full game sessions. The sample sizes are n = 42, n = 42 (Carbamazepine: rest, full game), n = 24, n = 24 (Phenytoin: rest, full game), n = 24, n = 23 (Perampanel: rest, full game), n = 354, n = 400 (Control: rest, full game). b, e, h) Post-hoc Games-Howell test between all the rest and all the full game groups. >: x > y by significance level and <: x <y by significance level. c, f, i) The same metrics calculated for different doses of each drug. The sample sizes are n = 12, n = 12; n = 6, n = 6; n = 24, n = 24 (Carbamazepine: rest, full game), n = 12, n = 12, n = 12, n = 12 (Phenytoin: rest, full game), n = 12, n = 11; n = 12 , n = 12 (Perampanel: rest, full game) from low dose to high dose respectively. One-way ANOVA test withing each group and post-hoc Games Howell test between all the rest and all the full game groups of different doses. # or * indicate p<0.05, ## or ** indicate p<0.01, ### or *** indicate p< 0.001.*

Analysis of gameplay performance under control and pharmacological intervention conditions

To evaluate the game performance of cultures exposed to various pharmacological compounds, three distinct metrics were employed: Average Rally Length (representing the average number of accurate hits per rally), Hit/Miss Ratio (indicating the ratio of accurate hits to missed balls), and Aces to Game Ratio (illustrating the proportion of games where the ball is immediately missed after the initial serve, known as an ace). The distribution of these game performance metrics is depicted for all groups (Figure 5, a, d, g), and a statistical significance table is presented for comparing the mean values of different groups (Figure 5, b, e, h). Subsequently, the same metrics are computed for various doses of each administrated drug (Figure 5, c, f, i).

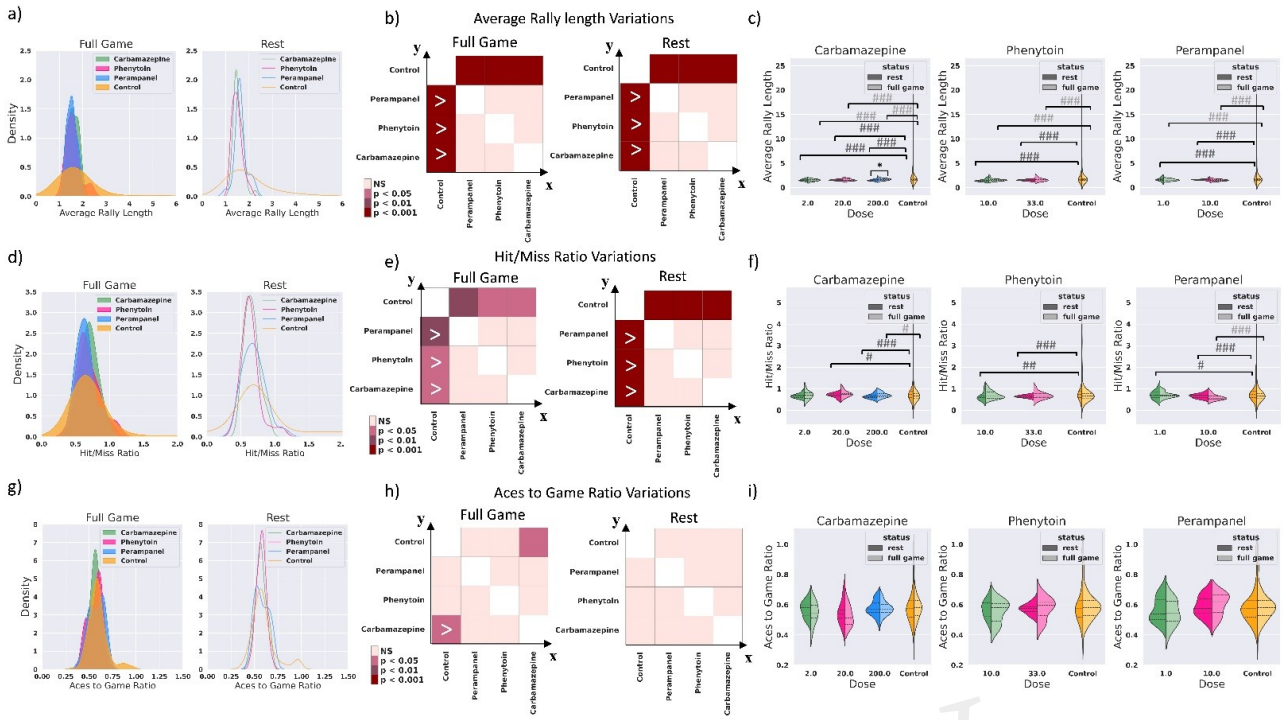

*Figure 5: Game performance analysis under control and pharmacological intervention conditions. a, d, g) Comparison of Average Rally Length, Hit/Miss Ratio, and Aces to Game Ratio in both rest and full game sessions. The sample sizes are n = 42, n = 42 (Carbamazepine: rest, full game), n = 24, n = 24 (Phenytoin: rest, full game), n = 24, n = 23 (Perampanel: rest, full game), n = 354, n = 400 (Control: rest, full game). b, e, h) Post-hoc Games-Howell test between all the rest and all the full game groups. >: x > y by significance level and <: x <y by significance level. c, f, i) The same metrics calculated for different doses of each drug. The sample sizes are n = 12, n = 12; n = 6, n = 6; n = 24, n = 24 (Carbamazepine: rest, full game), n = 12, n = 12, n = 12, n = 12 (Phenytoin: rest, full game), n = 12, n = 11; n = 12 , n = 12 (Perampanel: rest, full game) from low dose to high dose, respectively. One-way ANOVA test withing each group and post-hoc Games Howell test between all the rest and all the full game groups of different doses. # or * indicate p<0.05, ## or ** indicate p<0.01, ### or *** indicate p< 0.001.*

We next examined the effect of duration of gameplay on our analysis. Figure 6 (a, b, c) represents the percentage of changes in average rally length compared to rest under control and all the pharmacological interventions when studying the first and second half of each recording. The statistical significance table is presented for comparing the mean values of different groups in Figure 6 (d, e, f). High doses of Carbamazepine (200 μM) are the only group showing a significant improvement in time in terms of the average rally length compared to rest.

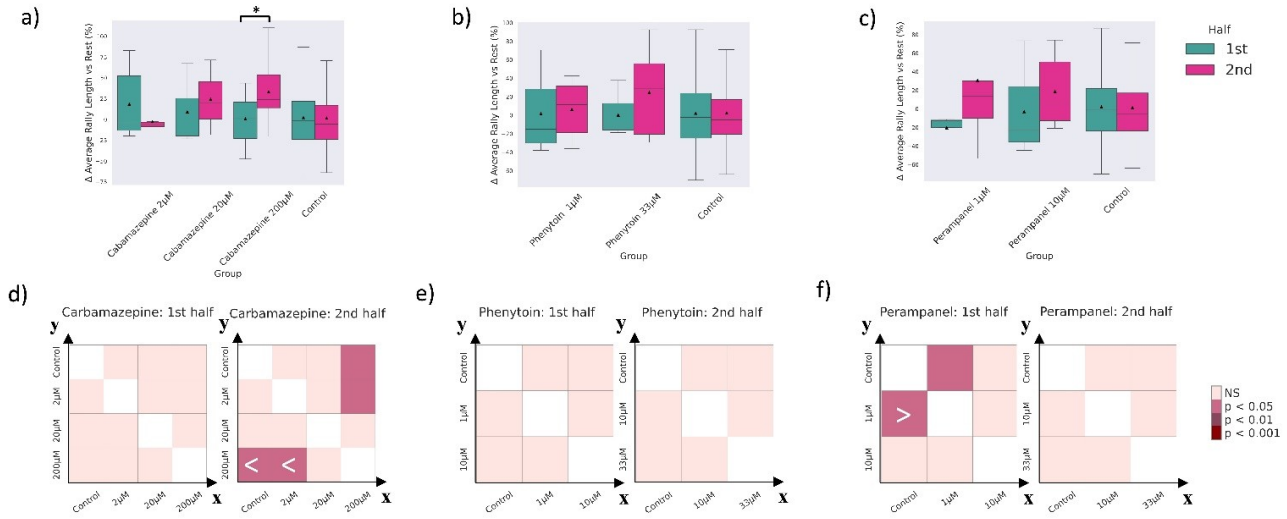

*Figure 6: Time-based game performance analysis under control and pharmacological intervention conditions. a, b, c) Comparison of Average Rally Length changes in full game sessions vs rest when comparing the first and second half of each recording. d, f, h) Post-hoc Games-Howell test between all the first and all the second half groups. >: x > y by significance level and <: x <y by significance level. * indicates p < 0.05.*

Bursting patterns of activity under control and pharmacological intervention conditions

Drawing inspiration from the burst classification methods outlined in (Wagenaar et al., 2006), we extracted quantitative details from the bursting patterns of the recordings from each *in vitro* culture.

In certain recordings, bursts displayed highly consistent sizes, while others exhibited a broad range of burst sizes. For each recording from a specific culture, N* denotes the number of spikes in the third-largest burst. Bursts containing at least 75% of N* spikes were categorized as large, those with at least 25% but less than 75% of N* spikes were deemed medium, and bursts containing fewer than 25% of N* spikes were labeled as small.

We proceeded to tally the number of small, medium, and large bursts in all recordings. Furthermore, we normalized the counts of various burst sizes in all subsequent sessions to the count of those burst sizes in the initial rest session recording.

Figure 7 (a, b, c) shows the number of extracted small, medium, and large bursts from full game and rest sessions under control and all the pharmacological interventions. Post-hoc statistical significance for the comparisons between groups are visually represented in Figure 7 (d, e, f). The same metrics are then illustrated for various administrated doses of each drug compared to the control group in Figure 7 (g-o).

The count of small bursts dropped significantly both during rest and gameplay with administration of all compounds. The count of large bursts also significant decreased in both Carbamazepine and Phenytoin groups during gameplay relative to control and significantly decreased in the Phenytoin and Perampanel-treated groups during rest compared to the control group.

In review

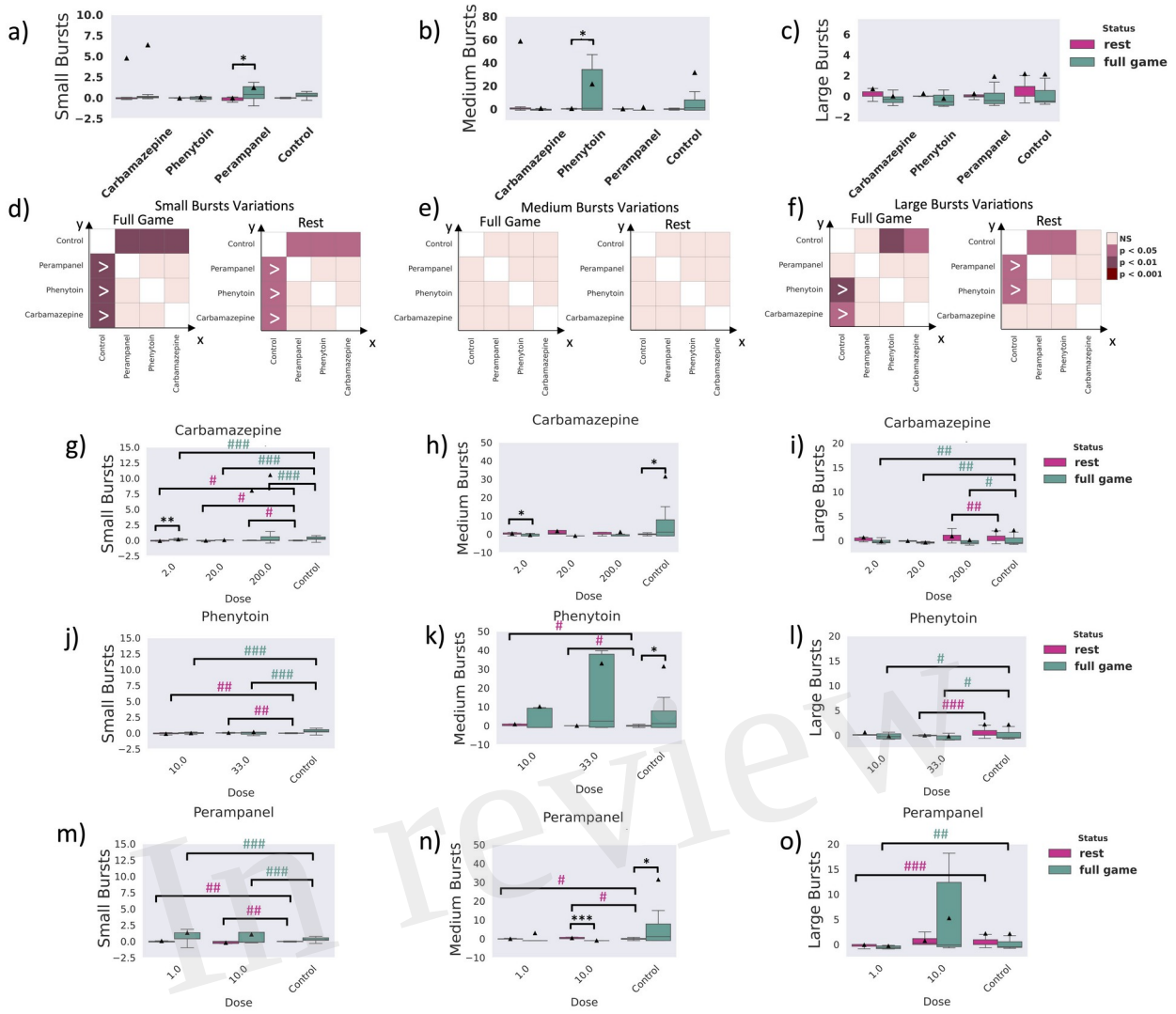

*Figure 7: Burst pattern analysis under control and pharmacological intervention conditions. a, b, c) The normalized number of small, medium, and large bursts for rest and full game sessions of all control and drug treated cultures. The first rest session recording of each experiment is used for normalization. The sample sizes are n = 35, n = 35 (Carbamazepine: rest, full game), n = 20, n = 20 (Phenytoin: rest, full game), n = 20, n = 20 (Perampanel: rest, full game), n = 97, n = 95 (Control: rest, full game) from left to right. One-way ANOVA test. d, e, f) Post-hoc Games-Howell test between all the rest and all the full game groups. >: x > y by significance level and <: x <y by significance level. g, h, i, j, k, l, m, n, o) Comparison of the same burst pattern metrics between different administrated doses of each drug. One-way ANOVA test within each group and post-hoc Tukey's test between all the rest and all the full game groups. # or * indicate p<0.05, ## or ** indicate p<0.01, ### or *** indicate p< 0.001.*

Figure 8 (a, c) shows the Pearson correlation values between each of the burst pattern metrics and different electrophysiological and game performance metrics including the metrics introduced previously. The corresponding *p*-values are illustrated in Figure 8 (b, d). Interestingly, the Mean Firing Rate appears to be negatively and significantly correlated with the number of small and large bursts in the cultures.

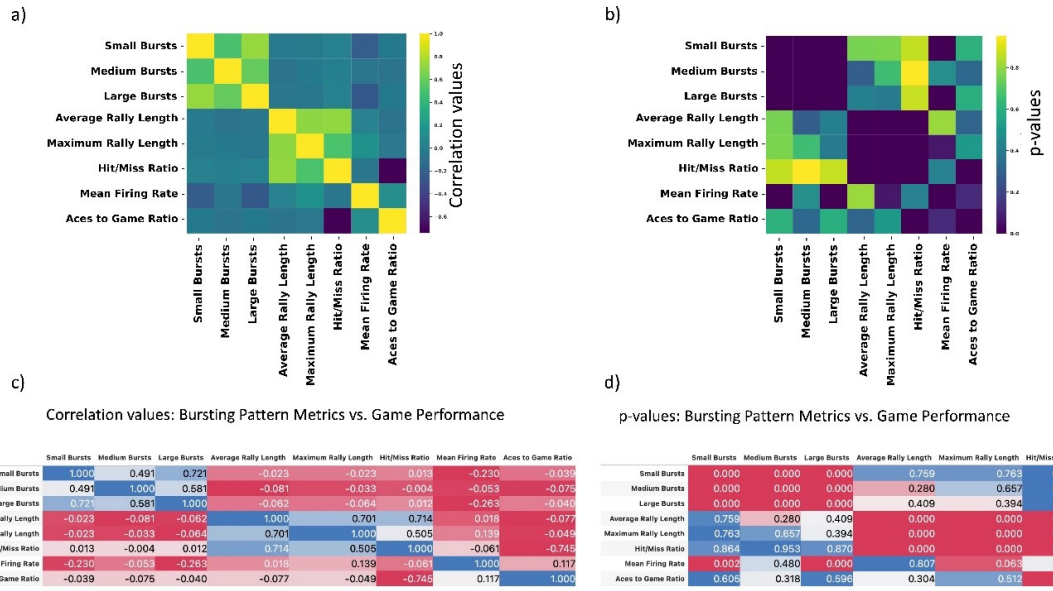

c)

Correlation values: Bursting Pattern Metrics vs. Game Performance

	Small Bursts	Medium Bursts	Large Bursts	Average Rally Length	Maximum Rally Length	Hit/Miss Ratio	Mean Firing Rate	Aces to Game Ratio
Small Bursts	1.000	0.491	0.721	-0.023	-0.023	0.013	-0.230	-0.039
Medium Bursts	0.491	1.000	0.581	-0.081	-0.033	-0.004	-0.053	-0.075
Large Bursts	0.721	0.581	1.000	-0.062	-0.064	0.012	-0.263	-0.040
Average Rally Length	-0.023	-0.081	-0.062	1.000	0.701	0.714	0.018	-0.077
Maximum Rally Length	-0.023	-0.033	-0.064	0.701	1.000	0.505	0.139	-0.049
Hit/Miss Ratio	0.013	-0.004	0.012	0.714	0.505	1.000	-0.061	-0.745
Mean Firing Rate	-0.230	-0.053	-0.263	0.018	0.139	-0.061	1.000	0.117
Aces to Game Ratio	-0.039	-0.075	-0.040	-0.077	-0.049	-0.745	0.117	1.000

d)

p-values: Bursting Pattern Metrics vs. Game Performance

	Small Bursts	Medium Bursts	Large Bursts	Average Rally Length	Maximum Rally Length	Hit/Miss Ratio	Mean Firing Rate	Aces to Game Ratio
Small Bursts	0.000	0.000	0.000	0.759	0.763	0.864	0.002	0.605
Medium Bursts	0.000	0.000	0.000	0.280	0.657	0.953	0.480	0.318
Large Bursts	0.000	0.000	0.000	0.409	0.394	0.870	0.000	0.596
Average Rally Length	0.759	0.280	0.409	0.000	0.000	0.000	0.807	0.304
Maximum Rally Length	0.763	0.657	0.394	0.000	0.000	0.000	0.063	0.512
Hit/Miss Ratio	0.864	0.953	0.870	0.000	0.000	0.000	0.419	0.000
Mean Firing Rate	0.002	0.480	0.000	0.807	0.063	0.419	0.000	0.116
Aces to Game Ratio	0.605	0.318	0.596	0.304	0.512	0.000	0.116	0.000

Figure 8: Pearson correlation test between the burst pattern and the game performance metrics. a, c) show the correlation values while b, d) report the corresponding p-values of the Pearson test.

In review

Critical dynamics of cultures under control and pharmacological intervention conditions

Dynamical systems undergo transitions between ordered and disordered states, and the concept of "criticality" emerges when the system resides at the boundary between these states—where the input is neither strongly damped nor excessively amplified. Failures in adaptive criticality may contribute to impairments in brain function, such as those observed in dementia or epilepsy. Building on insights from Habibollahi et al. (2023), an avalanche analysis was conducted to examine the network in relation to its proximity to criticality.

The start and end of an avalanche are determined by crossing a threshold of network activity, with spikes from any or all neurons within a specified region capable of triggering an avalanche. The scale-free dynamics of detected neuronal avalanches, along with metrics such as the Deviation from Criticality Coefficient (DCC), Branching Ratio (BR), and Shape Collapse error (SC error), were assessed to gauge whether the recordings were poised near criticality Habibollahi et al. (2023). A lower DCC and SC error, along with a BR closer to 1, serve as indicators of a state near criticality.

In this study, all these metrics were extracted for both gameplay and rest conditions under control, as well as for different applied doses of pharmacological interventions, as illustrated in Figure 9

Figure 9 (a, b, c) show the number of extracted DCC, BR, and SC error from full game and rest sessions under control and all the pharmacological interventions. Post-hoc statistical significance for the comparisons between groups are visually represented in Figure 9 (d, e, f). The same metrics are then illustrated for various administrated doses of each drug compared to the control group in Figure 9 (g-o).

The results demonstrate that criticality metrics are greatly disrupted both under control and pharmacological intervention in both game states. Some small variations are observed such as decreased DCC and increased BR values in low doses of Carbamazepine (2μM) or decreased SC error in higher doses (200μM) compared to control during gameplay. The BR also display a significant increase when comparing gameplay to rest state in 200μM Carbamazepine. Overall, there is limited expression of the various criticality metrics in these near pure glutamatergic neural cells which is supported by previous literature which showed that critical state dynamics arise from a balance of excitatory and inhibitory neuronal networks.

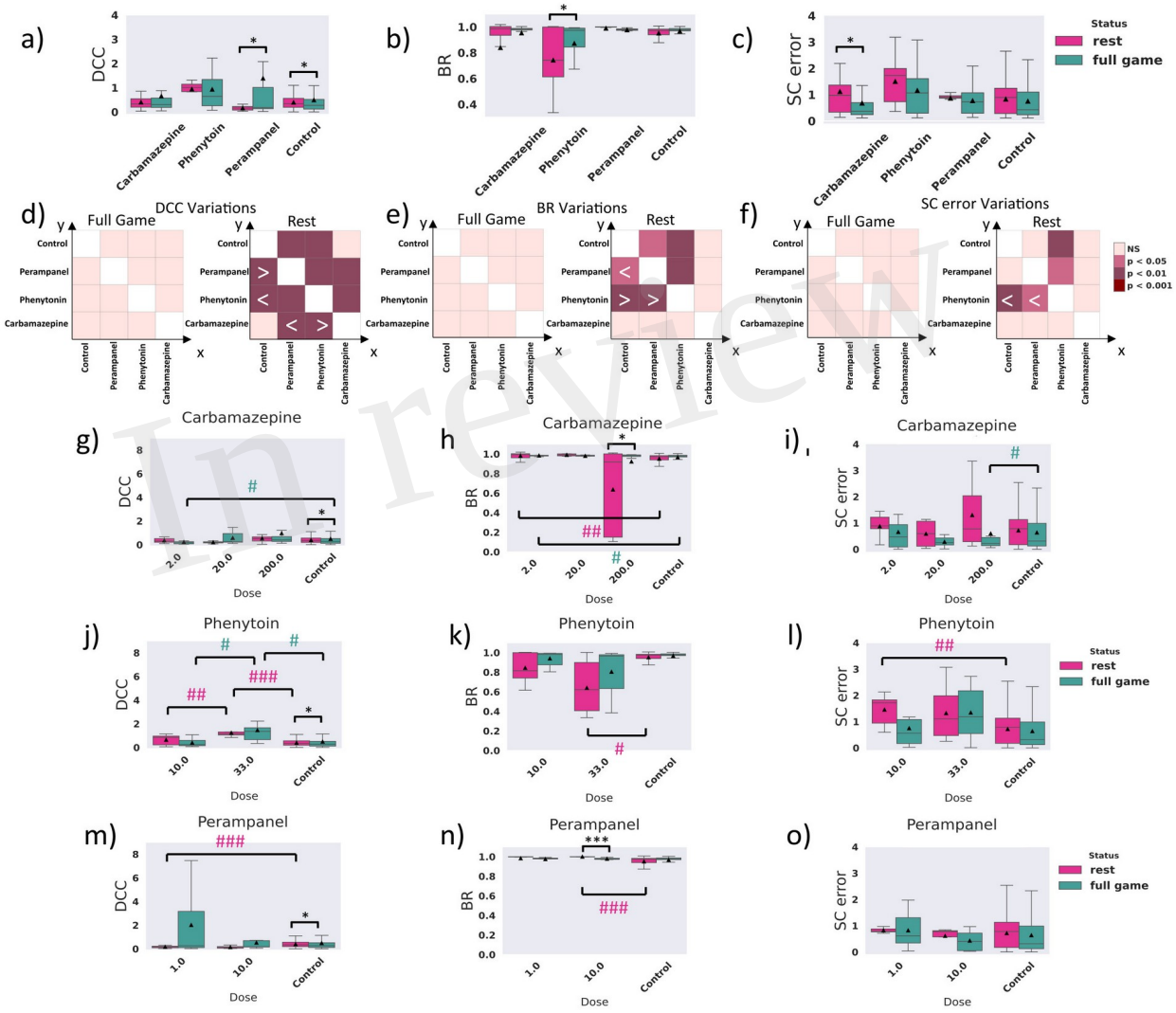

*Figure 9: Criticality analysis under control and pharmacological intervention conditions. a, b, c) The Deviation from Criticality Coefficient (DCC), Branching Ratio (BR), and Shape Collapse error (SC error) for rest and full game sessions of all control and drug treated cultures. The sample sizes are n = 24, n = 36 (Carbamazepine: rest, full game), n = 20, n = 24 (Phenytoin: rest, full game), n = 12, n = 19 (Perampanel: rest, full game), n = 288, n = 369 (Control: rest, full game) from left to right. One-way ANOVA test. d, e, f) Post-hoc Games-Howell test between all the rest and all the full game groups. >: x > y by significance level and <: x <y by significance level. g, h, i, j, k, l, m, n, o) Comparison of the same criticality metrics between different administrated doses of each drug. One-way ANOVA test withing each group and post-hoc Tukey's test between all the rest and all the full game groups. # or * indicate p<0.05, ## or ** indicate p<0.01, ### or *** indicate p< 0.001.*

Figure 10 (a, c) shows the Pearson correlation values between each of the criticality metrics and different electrophysiological and game performance metrics including the metrics introduced previously. The corresponding *p*-values are illustrated in Figure 10 (b, d). Culture game performance measured in Hit/Miss Ratio is negatively and significantly correlated with SC error while Mean Firing Rate appears to have a positive and significant correlation with this criticality metric.

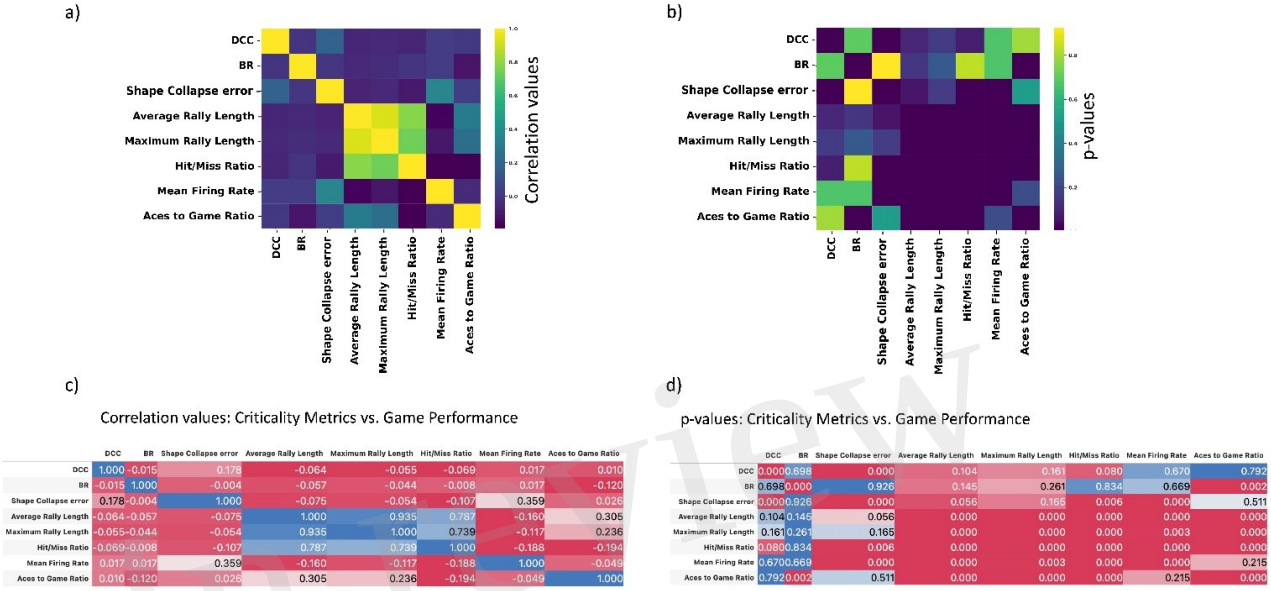

Figure 10: Pearson correlation test between the criticality and the game performance metrics. a, c) show the correlation values while b, d) report the corresponding p-values of the Pearson correlations.

Functional connectivity of cultures under control and pharmacological intervention conditions

In order to determine how ASD administration affected underlying network activity at rest and during gameplay, we used neuronal spiking activity to construct functional connectivity networks for all recordings. Due to the extensive duration of the recordings at a 20 kHz sampling frequency, the resulting time series data was substantial. Following the approach outlined in Khajehnejad et al. (2023), dimensionality reduction techniques, particularly t-SNE (Van der Maaten and Hinton, 2008), were employed to enhance computational efficiency and improve data interpretability. The 3-dimensional representations obtained using t-SNE for both rest and gameplay recordings were utilized to investigate latent network structures. Firstly, to assess the effectiveness of these low-dimensional representations, all recording sessions were divided in half before applying dimensionality reduction. Figure 11 (c, f, i, l) depicts these results after color labeling the first and second halves of the recording sessions for sample cultures during gameplay and rest conditions. The visualization shows that while the two halves of gameplay sessions are distinguishable using t-SNE, the distinction is less evident during rest sessions.

Functional connectivity network matrices were then constructed using zero-lag Pearson correlations for each gameplay or rest session recording, with the 1024 channels as nodes and weighted edges representing functional connectivity. Only edges with Pearson correlation absolute values above 0.7 were retained.

Considering that only a fraction of neurons fire at any given time within complex neural networks, inspired by Khajehnejad et al. (2023), a method was utilized to reduce computational complexity while preserving network dynamical properties. This involved identifying a subset of recorded channels that likely monitored neuronal populations specifically attuned to the ongoing task. Tucker decomposition via higher-order orthogonal iteration on tensor data from all lower-dimensional representations of the recordings was employed to identify a consistent subset of channels across all neuronal cultures. K-medoid clustering was then applied to partition the data into 30 clusters, and the corresponding 'medoids' were extracted as the mutual representative channels amongst all cultures.

Then, another network matrix using Pearson correlation was built with these 30 channels as nodes. The resulting functional connectivity networks were derived separately for the first and last 5 minutes of every recording.

Figure 11 (a-k) illustrate the heatmap of correlation values (i.e. edge weights) in the constructed functional connectivity networks for both the full network (1024 channels) and the smaller network (30 representative channels) and during rest and gameplay sessions.

In review

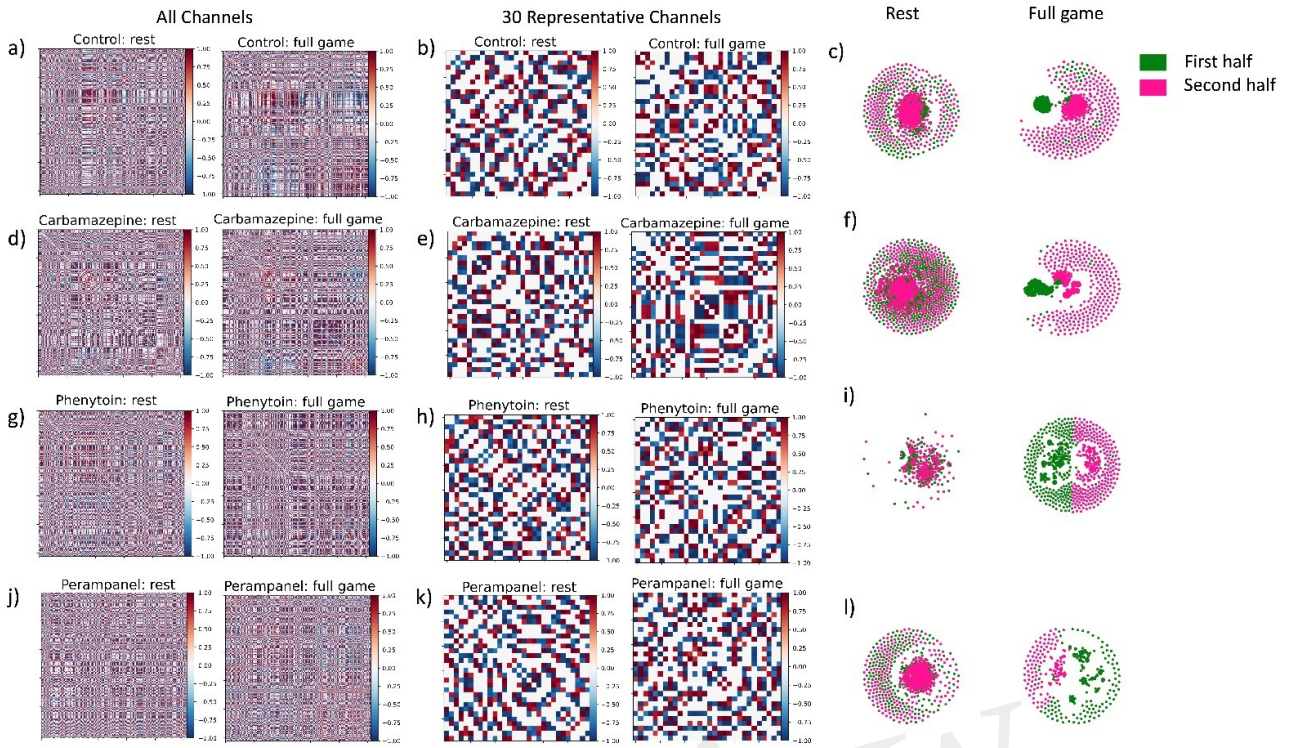

Figure 11: Functional connectivity networks of rest and gameplay sessions under control and pharmacological interventions. a-b, d-e, g-h, j-k) Heatmaps illustrating the average edge weights between all channels (on the left) or the 30 representative channels (on the right) in the Pearson Correlation network constructed from all rest and all full game recordings under control and pharmacological intervention conditions. The sample sizes are n = 42, n = 43 (Carbamazepine: rest, full game), n = 24, n = 24 (Phenytoin: rest, full game), n = 24, n = 24 (Perampanel: rest, full game), n = 354, n = 400 (Control: rest, full game). One-way ANOVA test. c, f, i, l) Low-dimensional representation of samples of rest and full game sessions using t-SNE under control and pharmacological intervention conditions (Carbamazepine, Phenytoin, and Perampanel, from top to bottom, respectively). The green and purple dots are the channel representations in the embedding space in the first and second halves of the recordings, respectively.

We then studied various macroscopic metrics of the connectivity network for the control group and all the different doses of the pharmacological interventions. The measured metrics encompassed:

1. Average Weight: This metric illustrates the mean value of Pearson Correlations calculated between pairs of spiking time series in each culture.

2. Modularity Index: This index quantifies the extent to which a network can be partitioned into distinct and internally cohesive groups or communities. It evaluates how nodes form clusters that are more densely connected within themselves than with nodes outside the cluster.

3. Clustering Coefficient: This measure quantifies the tendency of nodes to form clusters or highly connected groups, providing insights into the local connectivity of the network by assessing the likelihood that neighbours of a particular node are connected to each other.

Figure 12 represents these derived network metrics for the gameplay and rest sessions under pharmacological interventions and well as the control sessions.

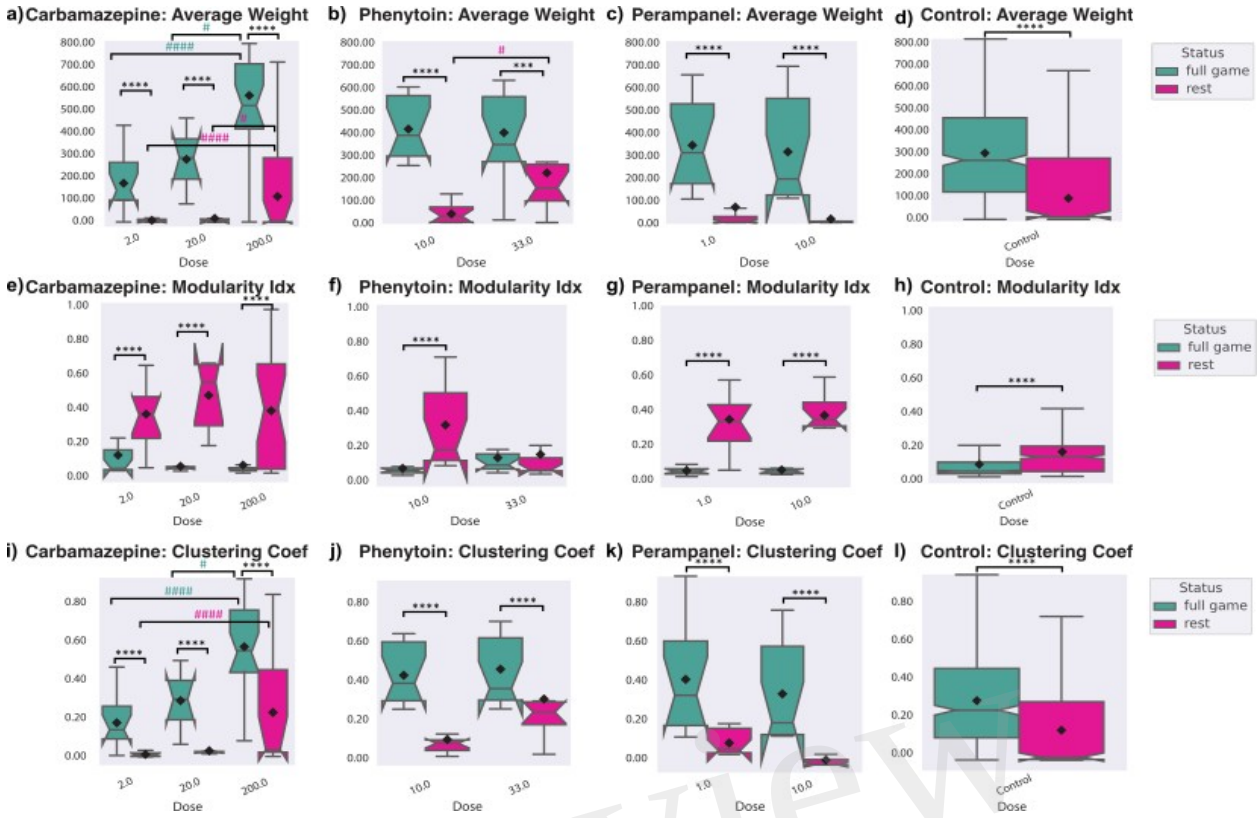

*Figure 12: Network summary statistics between gameplay and rest recordings using all of the recorded channels under control and different drug treatments. a, b, c, d) Average weight, e, f, g, h) Modularity Index, and i, j, k, l) Clustering coefficient values for gemeplay and rest recordings under control and all pharmacological interventions using the entire recording length from all 1024 recorded channels. One-way ANOVA test withing each group and post-hoc Tukey's test between all the rest and all the full game groups. # or * indicate p<0.05, ## or ** indicate p<0.01, ### or *** indicate p< 0.001.*

Next, to evaluate the dynamics of the functional connectivity networks in time, we divided each recording into 5 minute intervals and visualized the connectivity networks for the first and last 5 minutes of each group. Figure 13 represents these findings in both gameplay and rest sessions.

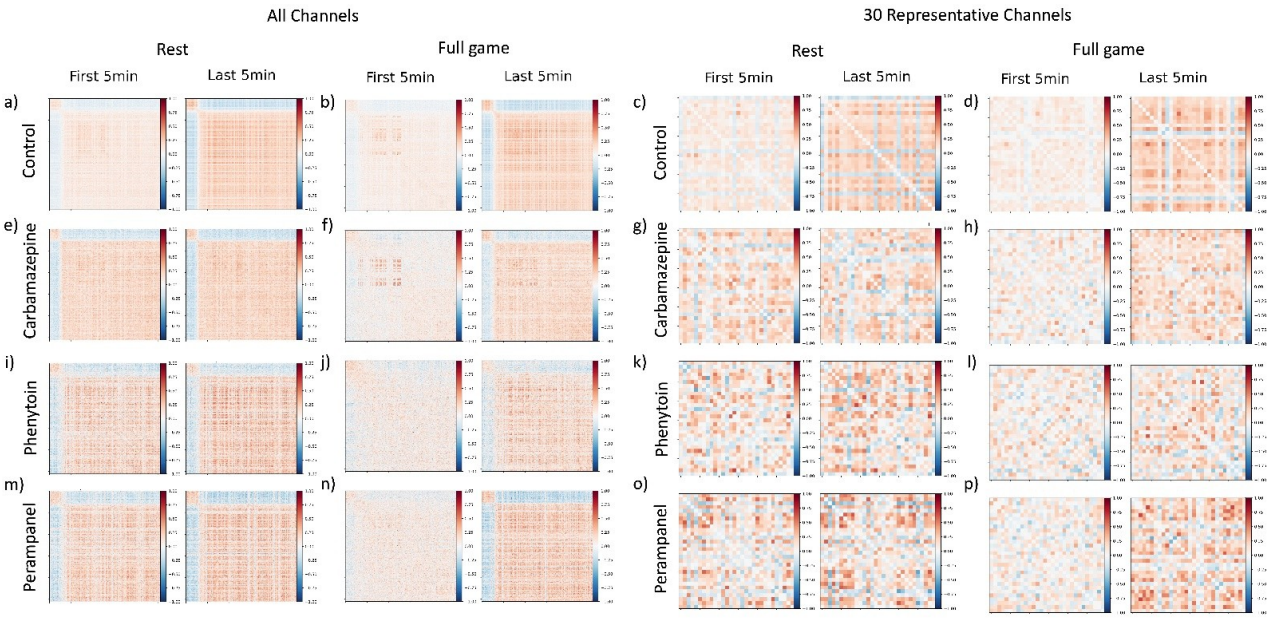

Figure 13: Changes in the functional connectivity networks of rest and gameplay sessions under control and pharmacological interventions. Heatmaps illustrate the change in average edge weights between (a-b, e-f, i-j, m-n) all channels or (c-d, g-h, k-l, o-p) the 30 representative channels in the Pearson Correlation network constructed from the first and last 5 minutes of all rest and all full game recordings under control and pharmacological intervention conditions.

In review

As a result of all pharmacological interventions, these functional connectivity networks using the low-dimensional representations of neural activity during rest and gameplay reveal distinct patterns evolving over time specifically during gameplay. This contrasts with the absence of such patterns during the spontaneous activity observed at rest. This difference is evident when considering both the full network (1024 channels; Figure 13, left panels) and the smaller network (30 representative channels; Figure 13, right panels).

We then studied the changes in the introduced macroscopic network metrics from pharmacological interventions when comparing the first and last 5 minutes of recordings. We utilise the first and last 5-minute time intervals, for both the full network and the smaller network.

Figure 14 and Supplementary Figure 1 represent the evolution of the macroscopic network metrics over time under the various pharmacological interventions using the full and the smaller networks, respectively. Figure 15 studies the same network statistics for various doses of administrated drugs. Carbamazepine appears to only show a significant change in network dynamics under its high dose administration (200 μM). Increasing average weight and clustering coefficient as well as decreasing modularity index is observed during gameplay but not in rest using all of the administrated drugs. While these differences in gameplay are more significant for Phenytoin and Perampanel, specifically using the full network in Figure 14, they rapidly lose the changes which arise during the initial embodiment in the gameplay environment and return to baseline levels observed during rest. This returning to baseline effect is not observed after Carbamazepine administration.

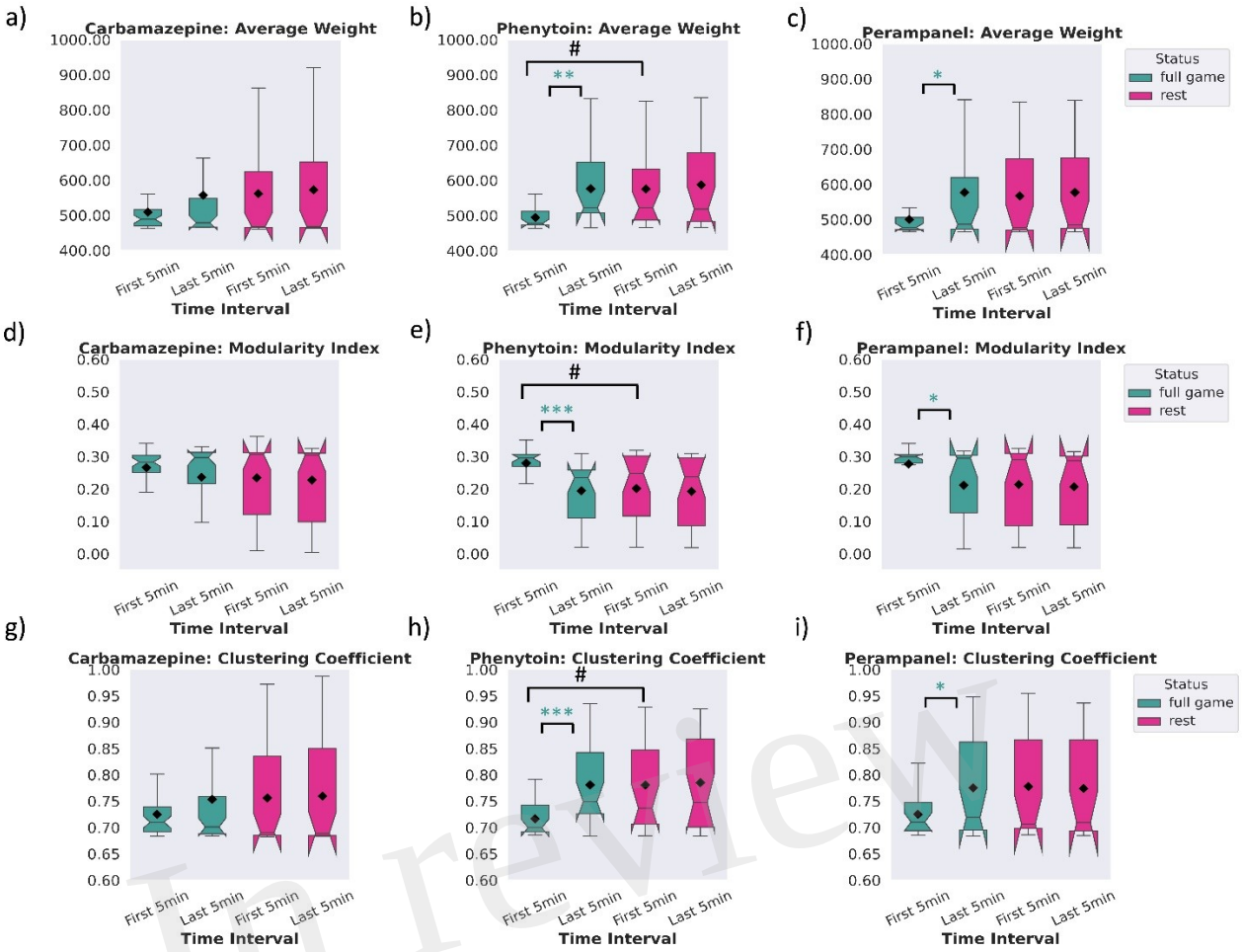

*Figure 14: Network summary statistics between the first and last 5 minutes of full game and rest recordings using all of the recorded channels under different drug treatments. a, b, c) Average weight, d, e, f) Modularity Index, and g, h, i) Clustering coefficient values for the first and last 5 minutes of recordings under all pharmacological intervention using all 1024 recorded channels. One-way ANOVA test withing each group and post-hoc Tukey's test between all the rest and all the full game groups. # or * indicate p<0.05, ## or ** indicate p<0.01, ### or *** indicate p< 0.001.*

In review

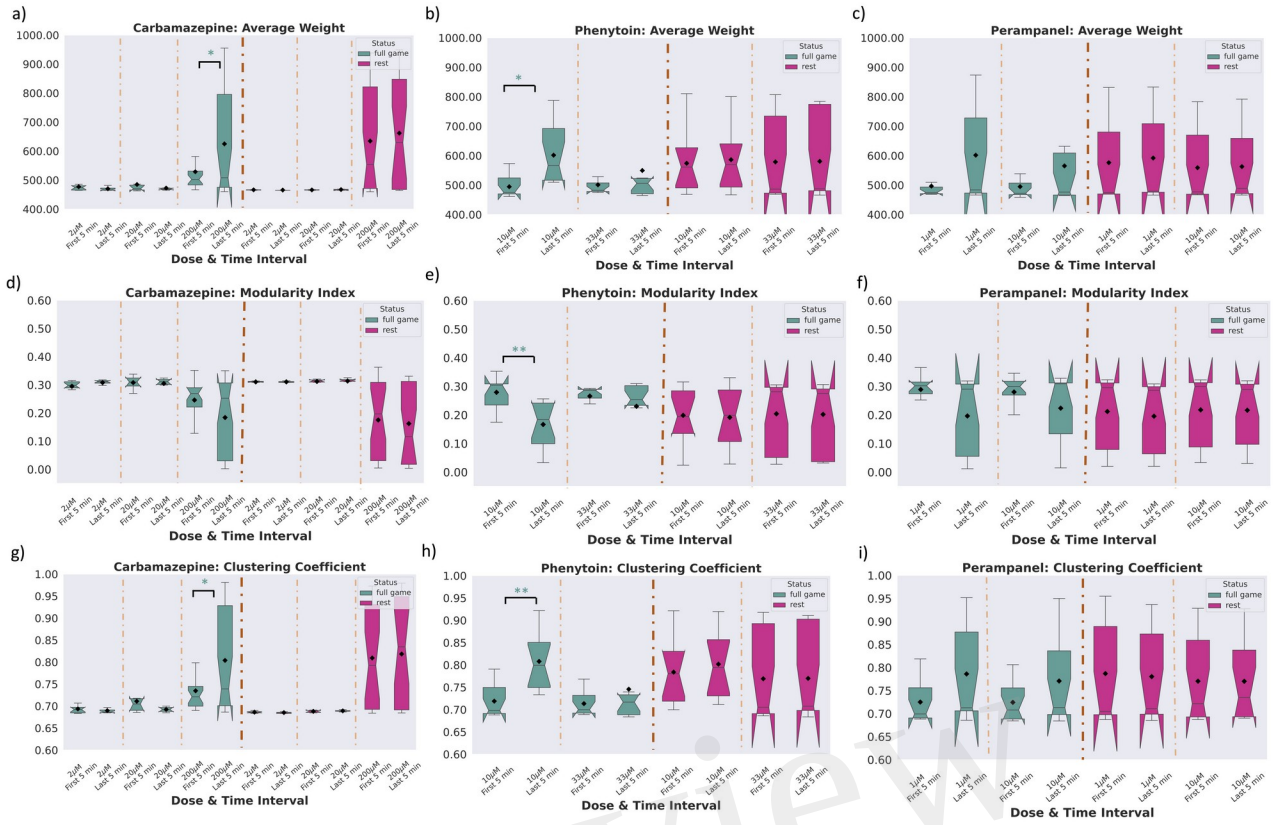

*Figure 15: Network summary statistics between the first and last 5 minutes of full game and rest recordings using all of the recorded channels under different doses of drug treatments. a, b, c) Average weight, d, e, f) Modularity Index, and g, h, i) Clustering coefficient values for the first and last 5 minutes of recordings under all doses of the pharmacological interventions using all 1024 recorded channels. One-way ANOVA test withing each group and post-hoc Tukey's test between all the rest and all the full game groups. * indicates p<0.05, ** indicates p<0.01, *** indicates p< 0.001.*

Discussion

Modelling dynamic environments through closed-loop electrophysiological stimulation and recording, provides a method to embody simple neural cultures in a simulated game-world and may offer additional information over existing drug-response assays. By using an *in vitro* epilepsy-like model characterised by glutamatergic hyperactivity, we intended to explore the behaviour of these cells in a structured information landscape and the impact of pharmacological interventions intended to suppress electrophysiological hyperactivity. Using the OPTi-OX system (Pawlowski et al., 2017), NGN2-iNeurons were generated, which displayed elevated levels of glutamatergic markers. These NGN2-iNeurons demonstrated heightened electrophysiological activity, greatly exceeding that of primary cortical rodent cultures and dorsal forebrain cultures intended to model healthy activity (Kagan et al., 2022b). It is also interesting to note that the activity of these inducible lines far exceeds the activity of NGN2 iNeuron cultures previously generated using viral methods and tested in the *DishBrain* system, which did show evidence of statistically significant learning over time without pharmacological intervention (Kagan et al., 2022b). Whether these results reflect a greater consistency of NGN2 overexpression with the OPTi-OX system relative to viral methods,

or instead that the OPTi-OX system results in similar transgene expression but with more hyperactivity in the resulting cultures, is difficult to conclusively determine here. Either way, these data suggest that OPTi-OX NGN2 iNeurons can produce a robust model of epilepsy-like glutamatergic hyperactivity (Galanopoulou et al., 2012; Nieto-Estévez and Hsieh, 2020; Negraes et al., 2021; Alaverdian et al., 2023). Further support for this model's functionality was observed in the compound-specific electrophysiological modulation achieved when various ASDs were introduced to the cultures.

Preliminary pharmacological treatments of these cultures showed a reduction in culture activity after an hour of exposure to ASDs. As expected, we observed concentration-response relationships between the dose of drugs administered, and mean culture firing rate, indicating the presence of the drug's respective receptor targets, and the sensitivity of the glutamatergic hyperexcitable phenotype to pharmacological manipulation. The mechanism of action of all three compounds tested is established: perampanel binds non-competitively and selectively to AMPA-type glutamate receptors (Patsalos, 2015), and both phenytoin and carbamazepine block voltage gated sodium channels on the surface of neuronal cell membranes (Kuo, 1998; Sun et al., 2006; Hakami, 2021). The effect of ASD administration is a reduction in abberent neuronal excitability associated with seizures leading to a decreased likelihood of depolarization and action potential. The reduction in firing rate we measured in this study is consistent with the mechanism of action these compounds display clinically, and led us to question if the acute drug effect would translate to modulation of gameplay performance in the *DishBrain* assay.

When examining the overall gameplay performance characteristics of the neural cultures, significantly more variance was observed in control cultures without pharmacological intervention. Despite this variation, the mean performance for cells, when treated with carbamazepine, was statistically improved (more hits, longer rallies, fewer aces) when compared to control cells and other treatment groups. Similarly, only the 200 μM carbamazepine group showed overall significantly higher performance on average rally length in gameplay compared to rest. This result becomes more pronounced when looking at learning over time instead of just between groups overall, consistent with previous work in this area (Kagan et al., 2022b). Despite these statistically significant differences, the effect sizes are notably smaller than in previous work. Moreover, no statistically significant learning effects were observed over time in untreated cultures. Given the substantially different electrophysiological profile of the NGN2-iNeurons tested in this work relative to the virally induced NGN2 cells tested previously, this may reflect the possibility that epilepsy-like hyperactivity is not conducive to information processing and learning. This is supported by the observation that these small but significant learning effects occurred after the loss of the majority of activity in the presence of 200 μM carbamazepine. If so, this would provide some support for the use of these cells as a disease model, in-line with previous work (Alaverdian

In review

et al., 2023). Alternatively, it may indicate that the previously validated *DishBrain* platform is not a suitable assay for these specific cells and that variations must be extensively titrated to determine a suitable learning protocol. These questions form an important direction for future research. Nonetheless, it is interesting to observe that learning effects correspond with the compound specific impact on electrophysiological activity. Carbamazepine showed the greatest reduction in activity compared to controls out of all compounds tested and likewise showed the greatest learning effect. Whilst we are unaware of differences in clinical efficacy (seizure recurrence or remission) for monotherapy of epilepsy (Nevitt et al., 2019), binding affinity at the sodium channel appears to be stronger with carbamazepine compared to phenytoin (Kuo et al., 1997) and may explain the differences in culture activity and learning outcomes seen in this system. Likewise, consistent trends over time were also observed following the administration of ASDs to the hyperactive cultures. Formally, this does support the predictive validity of the model as a useful tool to investigate information processing of hyperactive epilepsy-like neural cultures that showcase glutamatergic overexpression.

Moreover, extending beyond whether neural cultures showcased any overt evidence of improved gameplay performance, it is also interesting to compare and contrast different electrophysiological phenomena while cells are embodied in the structured information landscape vs engaged only in spontaneous activity. For example, looking at different sizes of network burst activity, Phenytoin appears to significantly increase medium bursts during gameplay, but not during rest, while Perampanel has a similar effect on small bursts. The influence of these effects across different dosages appears reasonably consistent and likely reflects key mechanistic insights into the nuances of a particular compound influences neural activity both with and without structured stimulation. Without the ability to embody neural cultures in these closed-loop systems, it would not be possible to extract this data, providing further evidence as to the utility of this approach for future studies. Examining simple pairwise correlations did not reveal a direct and obvious link between these bursting patterns and gameplay characteristics. However, future work focused on explaining these mechanisms could aim to build more nuanced computational models to understand whether the existence of any moderated or mediated pathways do exist. Similarly, previous work established that when neural systems intended to model healthy activity placed in a closed-loop structured information landscape would show significantly closer to critical dynamics compared to when engaged in spontaneous activity alone (Habibollahi et al., 2023). Given that criticality has been identified as a clinically relevant metric and is specifically associated with epileptiform activity, it was a meaningful metric to consider in this work as well (Arviv et al., 2016; Zimmern, 2020). Consistent with this previous literature, criticality was found to be greatly disrupted in these cultures, even though some small evidence of variations due to pharmacological intervention and game state was found. The limited expression of the various criticality metrics in these near pure

In review

glutamatergic neurons also supports previous literature which showed that critical state dynamics arise from a balance of excitatory and inhibitory neuronal networks (Van Vreeswijk and Sompolinsky, 1996; Poil et al., 2012). Thus, the lack of excitatory-inhibitory balance in this work may explain the limited observations of critical dynamics and learning effects, relative to previously reported levels (Habibollahi et al., 2023). Despite this, it can still be observed that correlations between some criticality and performance metrics had a significant relationship. While this was not replicated across all measures, it provides support for further consideration of critical dynamics as a marker of pre-clinical pharmacological intervention.

Finally, we also explored the functional connectivity within neural cultures both unstimulated and when embodied in the gameplay environment. Previous research has found that functional connectivity is linked to key behavioural changes within *in vitro* cultures when embodied in structured information landscapes (Cai et al., 2023; Khajehnejad et al., 2023). This work is replicated here using low-dimensional representations of neural activity. Clear differences can be observed during gameplay, which are not seen during the purely spontaneous activity displayed during rest. This represents a degree of reorganisation in neural cultures, even if such organisation does not extend towards robust metrics of improved gameplay performance. When examining the average edge weights, either looking at all channels or the condensed 30 representative channels, it is apparent that there exists far more structure in the changes occurring in the cultures during the gameplay compared to rest, where minimal structured changes appear. Nonetheless, while looking at the network summary statistics between different pharmacological interventions during gameplay and rest a more nuanced picture emerges. In particular, it appears that administration of either Phenyotin and Perampanel results in the average weight, modularity index, and clustering coefficient metrics rapidly losing the changes which arise during the initial embodiment in the gameplay closed-loop environment, and returning to baselines levels observed during rest. In contrast, Carbamazepine administration results in more stable networks that do not return to resting baseline. Future research using more controllable paradigms – ideally allowing for prolonged testing times – will be required to interpret these results and forms an important direction for future research. Providing mechanistic interpretations of nuanced changes observed in these dynamic systems exceeds the scope of this specific research. Despite this limitation, these results do showcase the utility of conducting pharmacological assays in neural cultures when assessing SBI characteristics in a closed-looped structured information landscape. While the preclinical relevance of the metrics, such as functional connectivity, are yet to be conclusively determined, the additional data provided by an SBI approach can allow future research to create more predictive models to better understand how neural cultures are influenced by pharmacological intervention.

In review

Apart from the specific limitations already discussed, this paper also acknowledges several notable general constrains. Foremost, the *in vitro* epilepsy-like model adopted for this paper is a 2-dimentional monolayer culture. While this allowed rapid generation and iterations in testing different pharmacological compounds at a reasonably high throughput, it's likely that this does not capture the more complex activity which occurs in epilepsy. The generation of 3-dimensional neural organoids in simulated information rich environments has previously been proposed as a method called Organoid Intelligence (OI) (Harris et al., 2018; Hartung et al., 2023; Smirnova et al., 2023). An OI approach may offer the ability to determine even more complex interactions between the neural systems and pharmacological interventions. Additionally, future work could also consider generating and evaluating *in vitro* models from donors who display genetically related forms of epilepsy (Miller et al., 2001; Tejavibulya and Sia, 2016). Another key limitation of this work is that of the limited time window that testing could be undertaken, as previously explored, the *DishBrain* setup allows for restricted testing periods as the heat generated by the MEA system results in evaporation and changes in osmolarity of the cell culture media. These changes eventually result in degradation of cell health and eventual cascades of cell death in the cultures. Future work should aim to use systems that either generate minimal heat or adopt an approach of embedding neural cultures in closed-system perfusion circuits capable of a constant homeostatic control of the cell culturing environment. Further, while the drugs and doses chosen for this study represent established options for the treatment of epilepsy and have been used in similar preclinical drug screens involving NGN2 iPSC-derived neurons (Zhao et al., 2023), a more comprehensive panel of ASDs can be identified, including those with differing mechanisms of action. As such, future work could utilise wider libraries of compounds to gain a deeper insight into the effects of suppression of neuronal excitability on this system. Finally, this work intended to use the previously validated *DishBrain* system, however this assay was not titrated on a disease-model. It is possible that using different stimulation or recording settings might yield different performance outcomes. Future work should aim to use more modifiable systems capable trialling different learning environments and being able to iterate through different stimulation and recording assays rapidly.

Ultimately this work aimed to explore the utility of induced NGN2 neural cultures as a simple *in vitro* epilepsy model with a focus on glutamatergic hyperexcitability. Such cultures displayed strong electrophysiological activity along with an overexpression of glutamatergic markers. It was specifically hypothesized that the NGN2 cultures would show increased gameplay performance and closer to phenotypically normal electrophysiological population dynamics following the administration of appropriate pharmacological interventions. This hypothesis was supported, as gameplay performance improved upon administration of ASD pharmaceuticals consistent with the observed suppression of activity achieved in a compound specific manner. The use of a closed-loop

In review

real-time system of electrophysiological stimulation and recording to test the learning processes of these neural cultures within a simulated game-world under different conditions, provided significantly more information than through standard *in vitro* pre-clinical methods. While substantial future research is required to refine these models and improve the hardware, software, and wetware (cell culturing) over that used in these assays, this study does robustly support the utility of an SBI approach to testing the pre-clinical potential of pharmaceutical interventions. Despite these limitations, by testing this method to better capture the key functionality of neural systems (i.e., information processing), it has been possible to showcase how additional information not available with traditional techniques can be extracted. In the future, this approach could potentially demonstrate enhanced predictability for clinical trial data, paving the way for pre-clinical compound validation in a relevant human model system.

References

Alaverdian, D., Corradi, A. M., Sterlini, B., Benfenati, F., Murru, L., Passafaro, M., et al. (2023). Modeling PCDH19 clustering epilepsy by Neurogenin 2 induction of patient-derived induced pluripotent stem cells. *Epileptic. Disord.* 25, 371–382. doi: 10.1002/epd2.20065.

Arviv, O., Medvedovsky, M., Sheintuch, L., Goldstein, A., and Shriki, O. (2016). Deviations from Critical Dynamics in Interictal Epileptiform Activity. *J. Neurosci.* 36, 12276–12292. doi: 10.1523/JNEUROSCI.0809-16.2016.

Cai, H., Ao, Z., Tian, C., Wu, Z., Liu, H., Tchieu, J., et al. (2023). Brain organoid reservoir computing for artificial intelligence. *Nat. Electron.* 6, 1032–1039. doi: 10.1038/s41928-023-01069-w.

Campos, G., Fortuna, A., Falcão, A., and Alves, G. (2018). In vitro and in vivo experimental models employed in the discovery and development of antiepileptic drugs for pharmacoresistant epilepsy. *Epilepsy Res.* 146, 63–86. doi: 10.1016/j.eplepsyres.2018.07.008.

Galanopoulou, A. S., Buckmaster, P. S., Staley, K. J., Moshé, S. L., Perucca, E., Engel Jr, J., et al. (2012). Identification of new epilepsy treatments: issues in preclinical methodology. *Epilepsia* 53, 571–582.

Ghaderi, P., Marateb, H. R., and Safari, M.-S. (2018). Electrophysiological Profiling of Neocortical Neural Subtypes: A Semi-Supervised Method Applied to in vivo Whole-Cell Patch-Clamp Data. *Front. Neurosci.* 12, 823. doi: 10.3389/fnins.2018.00823.

Golyala, A., and Kwan, P. (2017). Drug development for refractory epilepsy: the past 25 years and beyond. *Seizure* 44, 147–156.

Habibollahi, F., Kagan, B. J., Burkitt, A. N., and French, C. (2023). Critical dynamics arise during structured information presentation within embodied in vitro neuronal networks. *Nat. Commun.* 14, 5287. doi: 10.1038/s41467-023-41020-3.

Hakami, T. (2021). Neuropharmacology of Antiseizure Drugs. *Neuropsychopharmacol. Rep.* 41, 336–351. doi: 10.1002/npr2.12196.

Harris, G., Eschment, M., Orozco, S. P., McCaffery, J. M., Maclennan, R., Severin, D., et al. (2018). Toxicity, recovery, and resilience in a 3D dopaminergic neuronal in vitro model exposed to rotenone. *Arch. Toxicol.* 92, 2587–2606. doi: 10.1007/s00204-018-2250-8.

In review

Hartung, T., Smirnova, L., Morales Pantoja, I. E., Akwaboah, A., Alam El Din, D.-M., Berlinicke, C. A., et al. (2023). The Baltimore declaration toward the exploration of organoid intelligence. *Front. Sci.* 1, 1068159. doi: 10.3389/fsci.2023.1068159.

Ho, S.-M., Hartley, B. J., Tcw, J., Beaumont, M., Stafford, K., Slesinger, P. A., et al. (2016). Rapid Ngn2-induction of excitatory neurons from hiPSC-derived neural progenitor cells. *Methods* 101, 113–124. doi: 10.1016/j.ymeth.2015.11.019.

Kagan, B. J., Duc, D., Stevens, I., and Gilbert, F. (2022a). Neurons Embodied in a Virtual World: Evidence for Organoid Ethics? *AJOB Neurosci.* 13, 114–117. doi: 10.1080/21507740.2022.2048731.

Kagan, B. J., Gyngell, C., Lysaght, T., Cole, V. M., Sawai, T., and Savulescu, J. (2023). The technology, opportunities, and challenges of Synthetic Biological Intelligence. *Biotechnol. Adv.* 68, 108233. doi: 10.1016/j.biotechadv.2023.108233.

Kagan, B. J., Kitchen, A. C., Tran, N. T., Habibollahi, F., Khajehnejad, M., Parker, B. J., et al. (2022b). In vitro neurons learn and exhibit sentience when embodied in a simulated game-world. *Neuron*, S0896627322008066. doi: 10.1016/j.neuron.2022.09.001.

Khajehnejad, M., Habibollahi, F., Loeffler, A., Kagan, B., and Razi, A. (2023). On Complex Network Dynamics of an In-Vitro Neuronal System during Rest and Gameplay. in *NeurIPS 2023 Generative AI and Biology (GenBio) Workshop*.

Kuo, C.-C. (1998). A Common Anticonvulsant Binding Site for Phenytoin, Carbamazepine, and Lamotrigine in Neuronal Na+ Channels. *Mol. Pharmacol.* 54, 712–721.

Kuo, C.-C., Chen, R.-S., Lu, L., and Chen, R.-C. (1997). Carbamazepine Inhibition of Neuronal Na+ Currents: Quantitative Distinction from Phenytoin and Possible Therapeutic Implications. *Mol. Pharmacol.* 51, 1077–1083. doi: 10.1124/mol.51.6.1077.

Kwan, P., Schachter, S. C., and Brodie, M. J. (2011). Drug-resistant epilepsy. *N. Engl. J. Med.* 365, 919–926.

Ly, C., Middleton, J. W., and Doiron, B. (2012). Cellular and Circuit Mechanisms Maintain Low Spike Co-Variability and Enhance Population Coding in Somatosensory Cortex. *Front. Comput. Neurosci.* 6. doi: 10.3389/fncom.2012.00007.

Miladinovic, T., Nashed, M., and Singh, G. (2015). Overview of Glutamatergic Dysregulation in Central Pathologies. *Biomolecules* 5, 3112–3141. doi: 10.3390/biom5043112.

Mileva, G., Zysman, D., Groothuis, S., and Lewis, J. E. (2008). In vitro studies of closed-loop feedback and electrosensory processing in Apteronotus leptorhynchus. *J. Physiol.-Paris* 102, 173–180. doi: 10.1016/j.jphysparis.2008.10.012.

Miller, M. C., Mohrenweiser, H. W., and Bell, D. A. (2001). Genetic variability in susceptibility and response to toxicants. *Toxicol. Lett.*, 12.

Negraes, P. D., Trujillo, C. A., Yu, N.-K., Wu, W., Yao, H., Liang, N., et al. (2021). Altered network and rescue of human neurons derived from individuals with early-onset genetic epilepsy. *Mol. Psychiatry* 26, 7047–7068. doi: 10.1038/s41380-021-01104-2.

Nevitt, S. J., Marson, A. G., and Tudur Smith, C. (2019). Carbamazepine versus phenytoin monotherapy for epilepsy: an individual participant data review. *Cochrane Database Syst. Rev.* 2019, CD001911. doi: 10.1002/14651858.CD001911.pub4.

In review

Nieto-Estévez, V., and Hsieh, J. (2020). Human Brain Organoid Models of Developmental Epilepsies. *Epilepsy Curr.* 20, 282–290. doi: 10.1177/1535759720949254.

Patsalos, P. N. (2015). The clinical pharmacology profile of the new antiepileptic drug perampanel: A novel noncompetitive AMPA receptor antagonist. *Epilepsia* 56, 12–27. doi: 10.1111/epi.12865.

Pawlowski, M., Ortmann, D., Bertero, A., Tavares, J. M., Pedersen, R. A., Vallier, L., et al. (2017). Inducible and Deterministic Forward Programming of Human Pluripotent Stem Cells into Neurons, Skeletal Myocytes, and Oligodendrocytes. *Stem Cell Rep.* 8, 803–812. doi: 10.1016/j.stemcr.2017.02.016.

Poil, S.-S., Hardstone, R., Mansvelder, H. D., and Linkenkaer-Hansen, K. (2012). Critical-State Dynamics of Avalanches and Oscillations Jointly Emerge from Balanced Excitation/Inhibition in Neuronal Networks. *J. Neurosci.* 32, 9817–9823. doi: 10.1523/JNEUROSCI.5990-11.2012.

Putnam, T. J., and Merritt, H. H. (1937). Experimental determination of the anticonvulsant properties of some phenyl derivatives. *Science* 85, 525–526.

Shahaf, G., and Marom, S. (2001). Learning in Networks of Cortical Neurons. *J. Neurosci.* 21, 8782–8788. doi: 10.1523/JNEUROSCI.21-22-08782.2001.

Smirnova, L., Caffo, B. S., Gracias, D. H., Huang, Q., Morales Pantoja, I. E., Tang, B., et al. (2023). Organoid intelligence (OI): the new frontier in biocomputing and intelligence-in-a-dish. *Front. Sci.* 1. doi: 10.3389/fsci.2023.1017235.

Sun, G., Werkman, T. R., and Wadman, W. J. (2006). Kinetic changes and modulation by carbamazepine on voltage-gated sodium channels in rat CA1 neurons after epilepsy. *Acta Pharmacol. Sin.* 27, 1537–1546. doi: 10.1111/j.1745-7254.2006.00452.x.

Tejavibulya, N., and Sia, S. K. (2016). Personalized Disease Models on a Chip. *Cell Syst.* 3, 416–418. doi: 10.1016/j.cels.2016.11.002.

Van der Maaten, L., and Hinton, G. (2008). Visualizing data using t-SNE. *J. Mach. Learn. Res.* 9.

Van Vreeswijk, C., and Sompolinsky, H. (1996). Chaos in Neuronal Networks with Balanced Excitatory and Inhibitory Activity. *Science* 274, 1724–1726. doi: 10.1126/science.274.5293.1724.

Wagenaar, D., Pine, J., and Potter, S. (2006). An extremely rich repertoire of bursting patterns during the development of cortical cultures. *BMC Neurosci.* 7, 11. doi: 10.1186/1471-2202-7-11.

Zhao, C., Rollo, B., Shahid Javaid, M., Huang, Z., He, W., Xu, H., et al. (2023). An integrated in vitro human iPSCs-derived neuron and in vivo animal approach for preclinical screening of anti-seizure compounds. *J. Adv. Res.* doi: 10.1016/j.jare.2023.11.022.

Zimmern, V. (2020). Why Brain Criticality Is Clinically Relevant: A Scoping Review. *Front. Neural Circuits* 14, 54. doi: 10.3389/fncir.2020.00054.

Conflict of Interest

BW, FH, CD, MK, AL, and BJK are employed by CCLABS Pty. Ltd., a for-profit company with an interest in the commercial viability of synthetic biological intelligence.

In review

Author Contributions

BW: Conception, Design, Data Acquisition, Data Analysis, Manuscript Preparation, Manuscript Review. FH: Data Analysis, Manuscript Preparation, Manuscript Review. CD: Data Acquisition, Manuscript Review. MKhaj: Data Analysis, Manuscript Preparation, Manuscript Review. AL: Data Analysis, Manuscript Preparation, Manuscript Review. KB: Design, Data Acquisition, Data Analysis, Manuscript Review. NP: Data Analysis, Manuscript Review. MKott: Conception, Manuscript Review. BJK: Conception, Design, Data Acquisition, Data Analysis, Manuscript Preparation, Manuscript Review.

Funding

CCLABS Pty Ltd. provided all funding for the equipment and reagents necessary for the completion of this work, except where otherwise noted in the text.

Acknowledgements

The authors wish to gratefully acknowledge the service and support of Dr. Irena (Iska) Carmichael and Monash Micro Imaging (Monash University, 6 Floor Burnet Tower, Alfred Research Alliance, 89 Commercial Rd, Melbourne, Australia, 3004) for their help in obtaining the immunocytochemistry images. Perampanel, as well as generous advice, was provided by Dr. Ben Rollo, Monash University, Melbourne, Australia.

In review

Supplementary Material

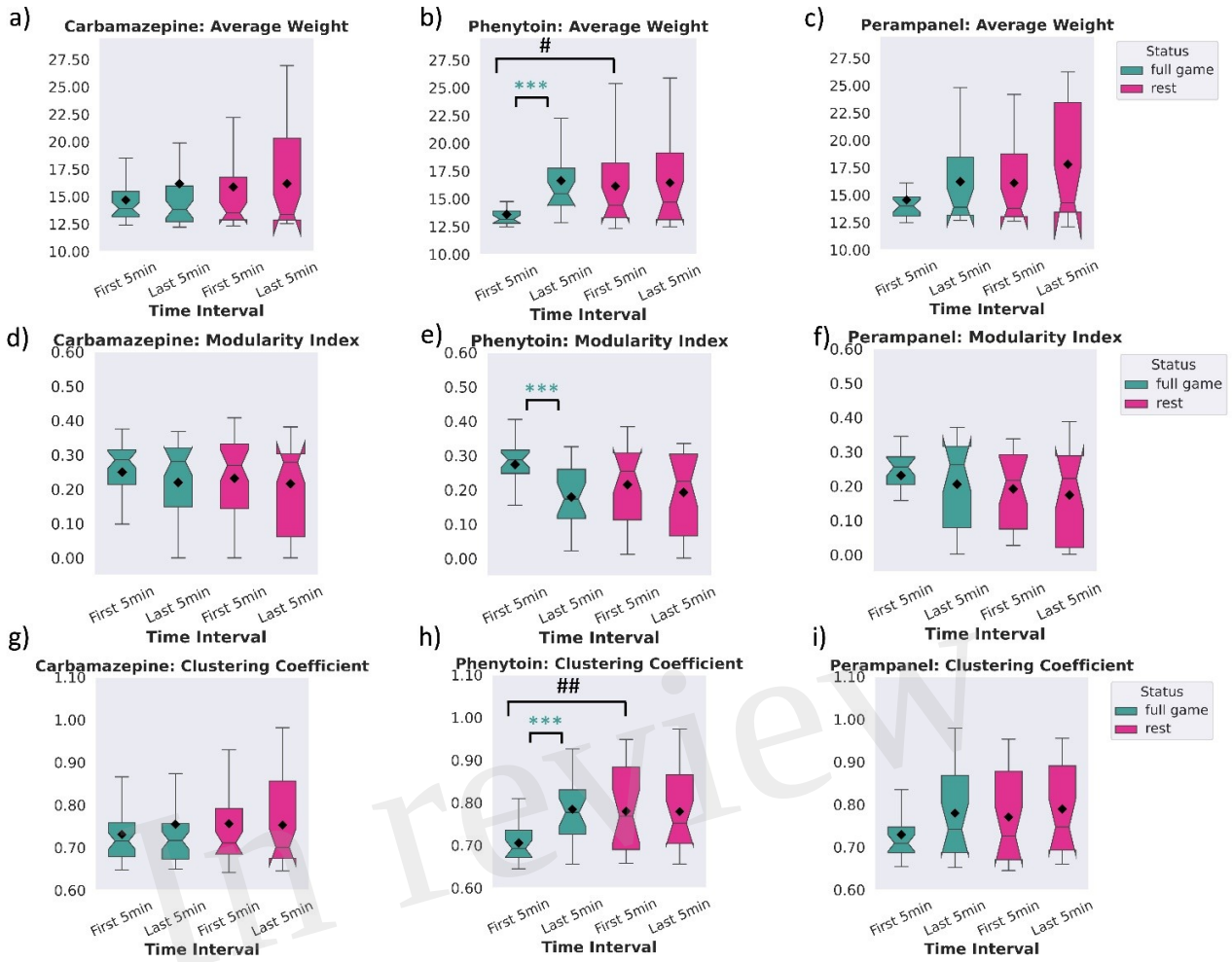

*Supplementary Figure 1: Network summary statistics between the first and last 5 minutes of full game and rest recordings using the 30 representative channels. a, b, c) Average weight, d, e, f) Modularity Index, and g, h, i) Clustering coefficient values for the first and last 5 minutes of recordings under all pharmacological intervention using the 30 representative channels. One-way ANOVA test withing each group and post-hoc Tukey's test between all the rest and all the full game groups. # or * indicate p<0.05, ## or ** indicate p<0.01, ### or *** indicate p< 0.001.*

Data Availability Statement

The imaging data in this study can be found in the figures; original high-res versions can be provided upon reasonable request. The raw RNA-Seq data files can be provided upon reasonable request. The electrophysiological datasets generated and analysed in this study can be found at the following repository: https://osf.io/xwf7v/?view_only=c731e5dbceeb4bf98032b9c5e0449e76.

In review

Figure 1.TIFF

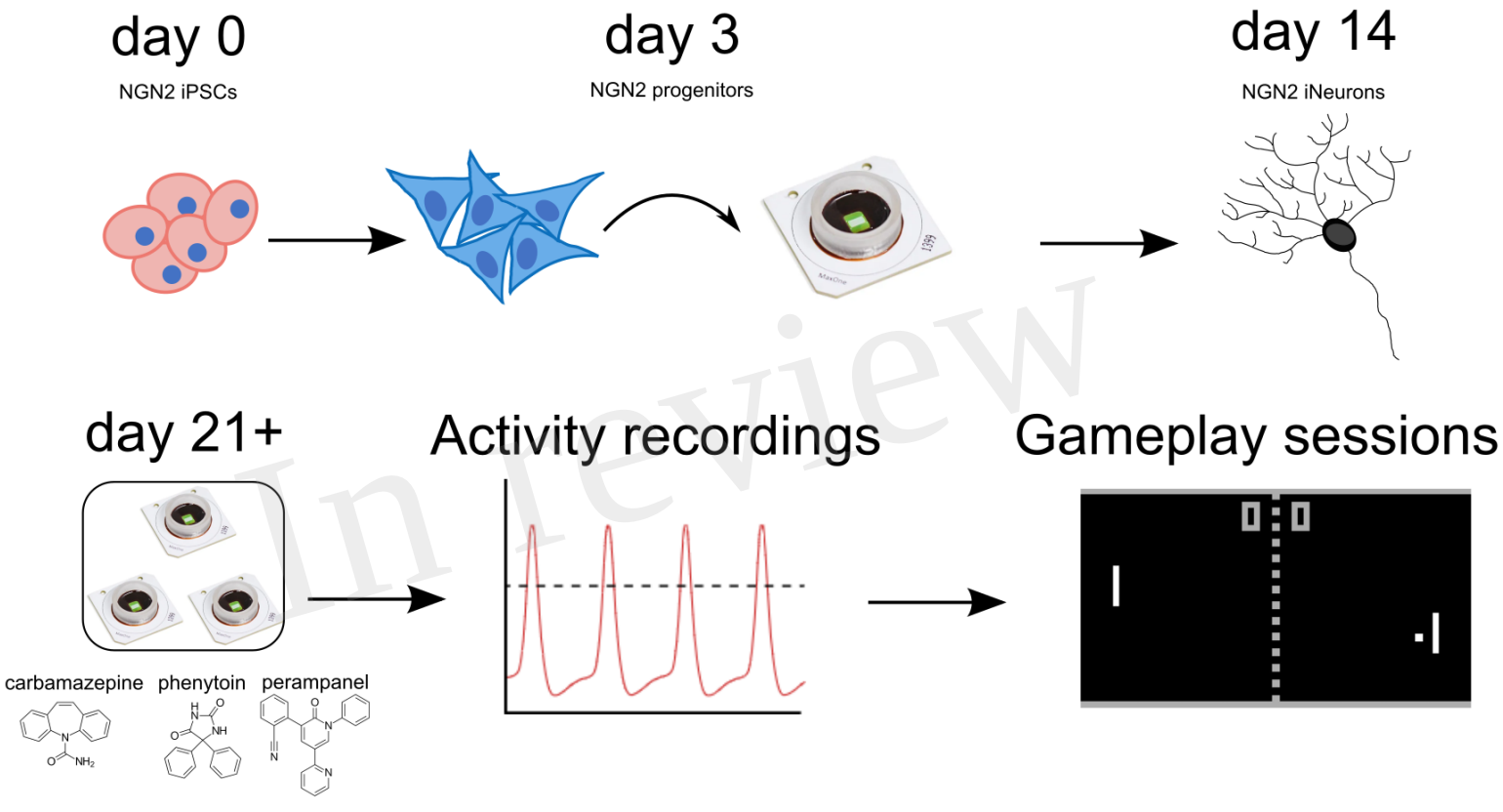

In review

Figure 2.TIFF

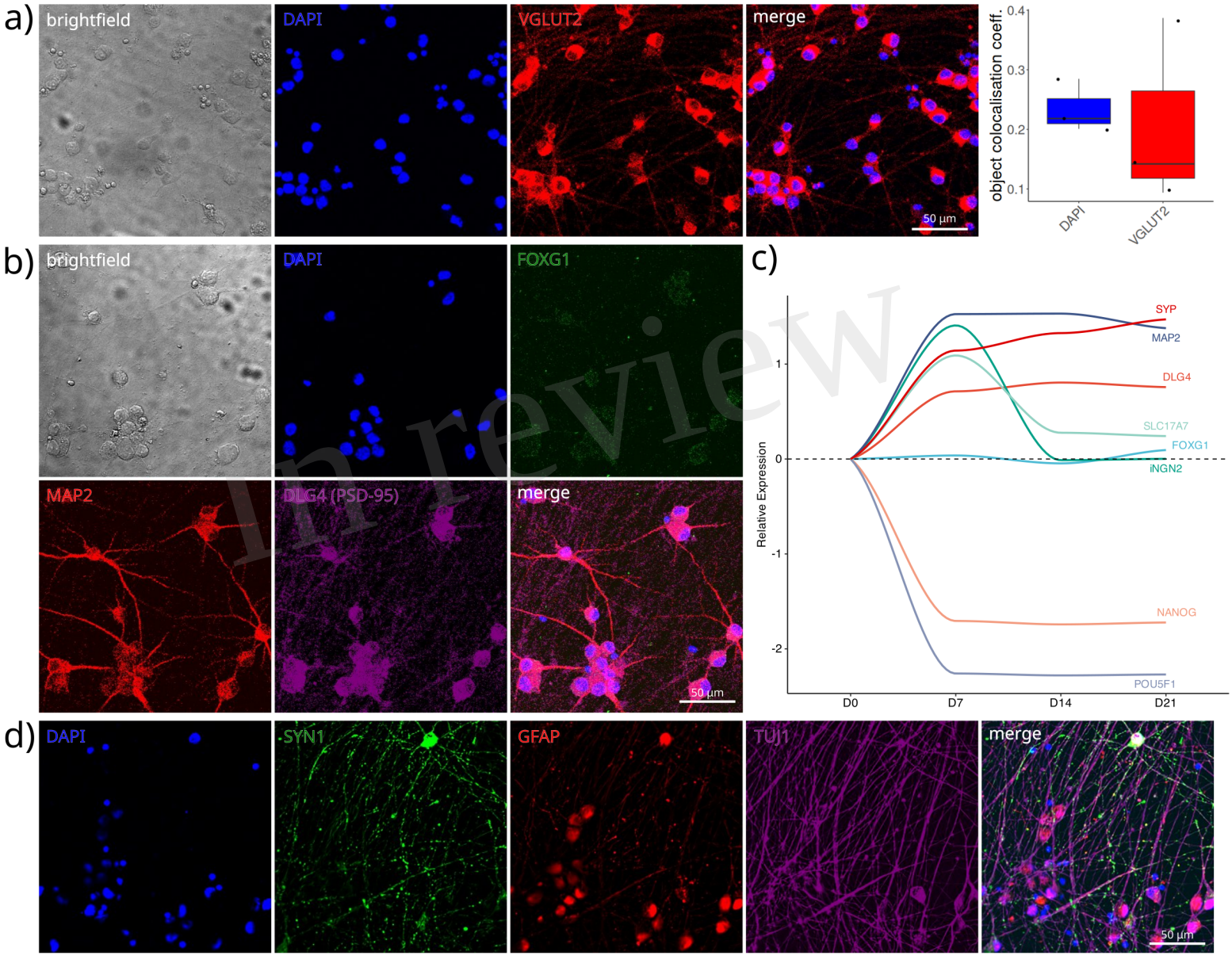

In review

Figure 3.TIFF

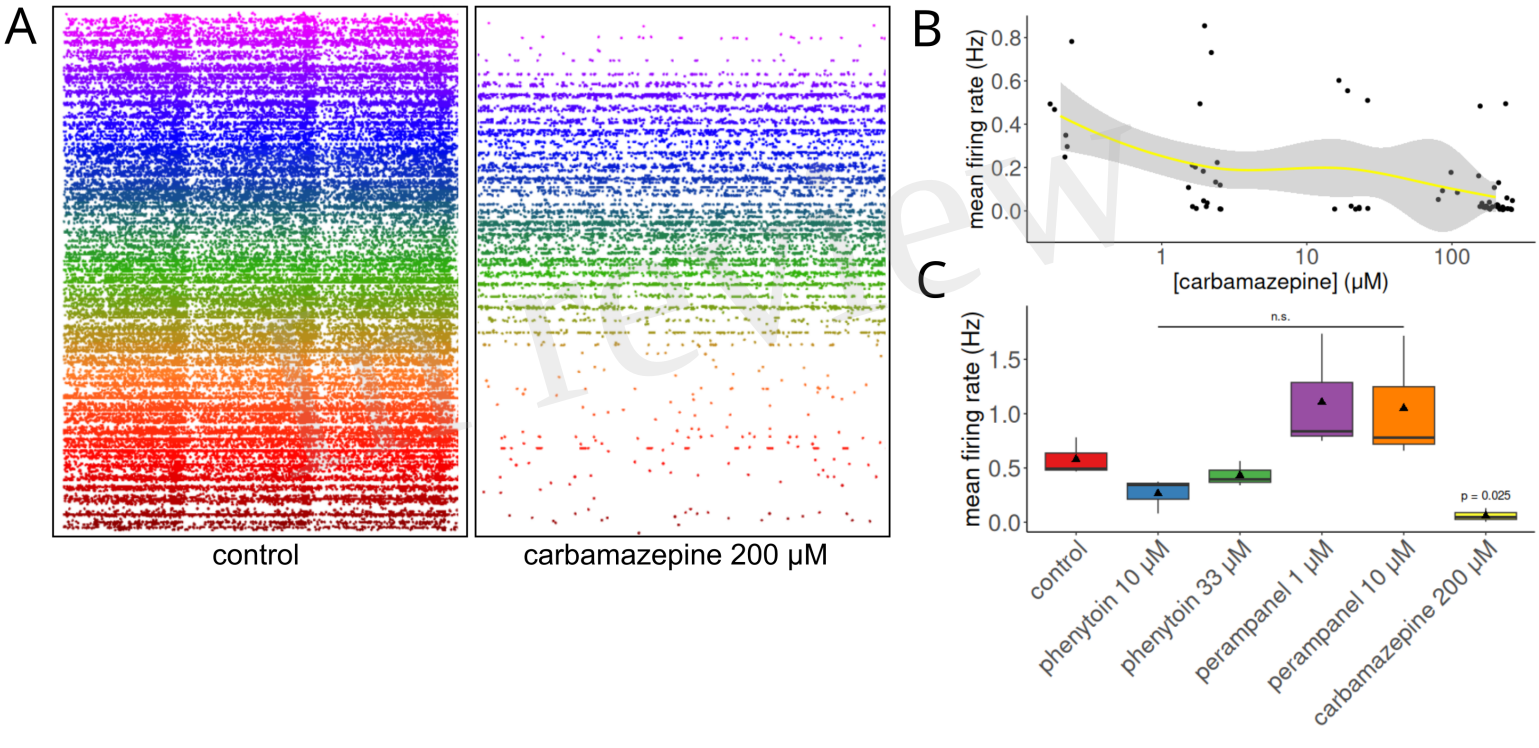

Figure 4.TIF

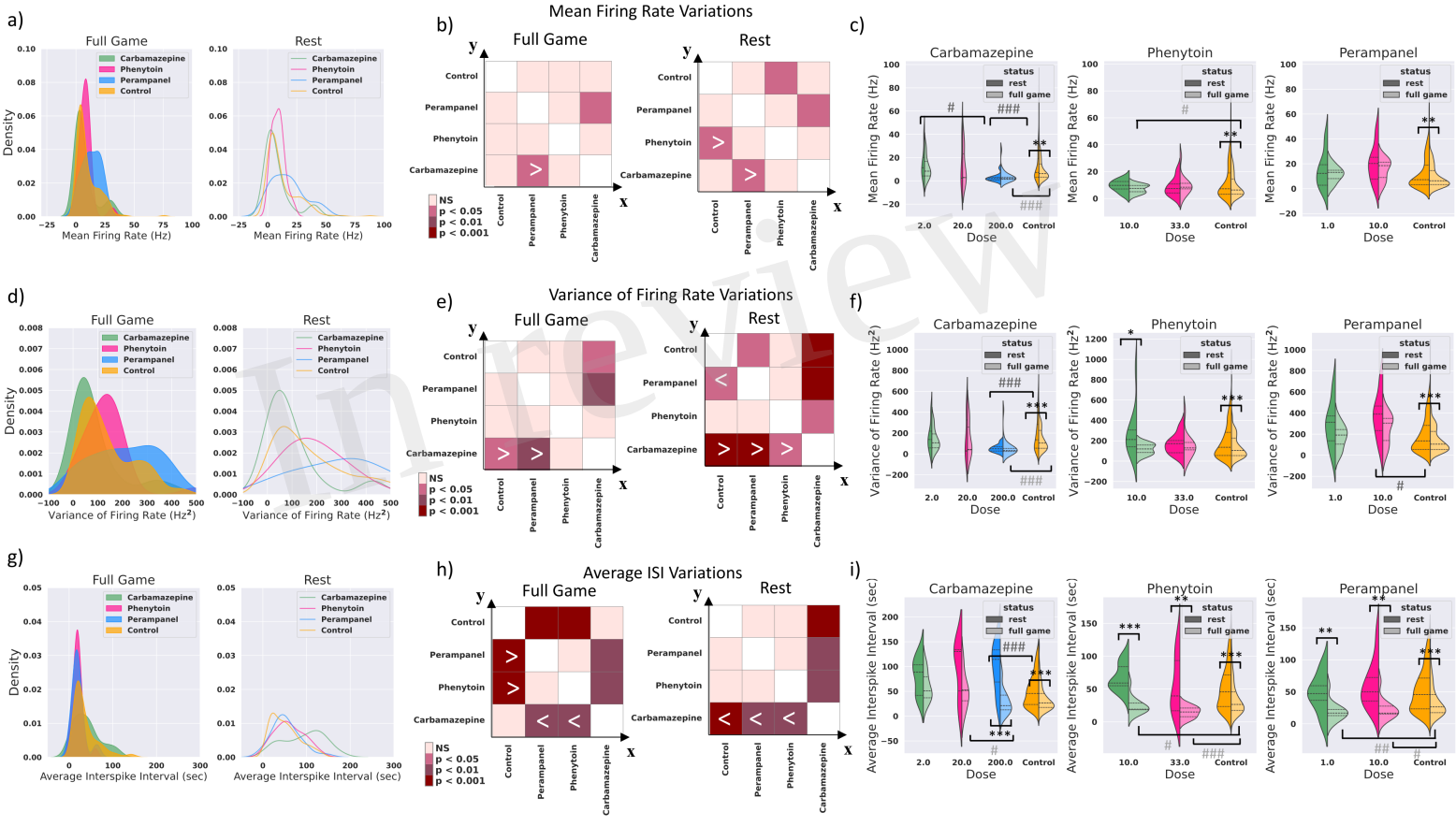

In review

Figure 5.TIF

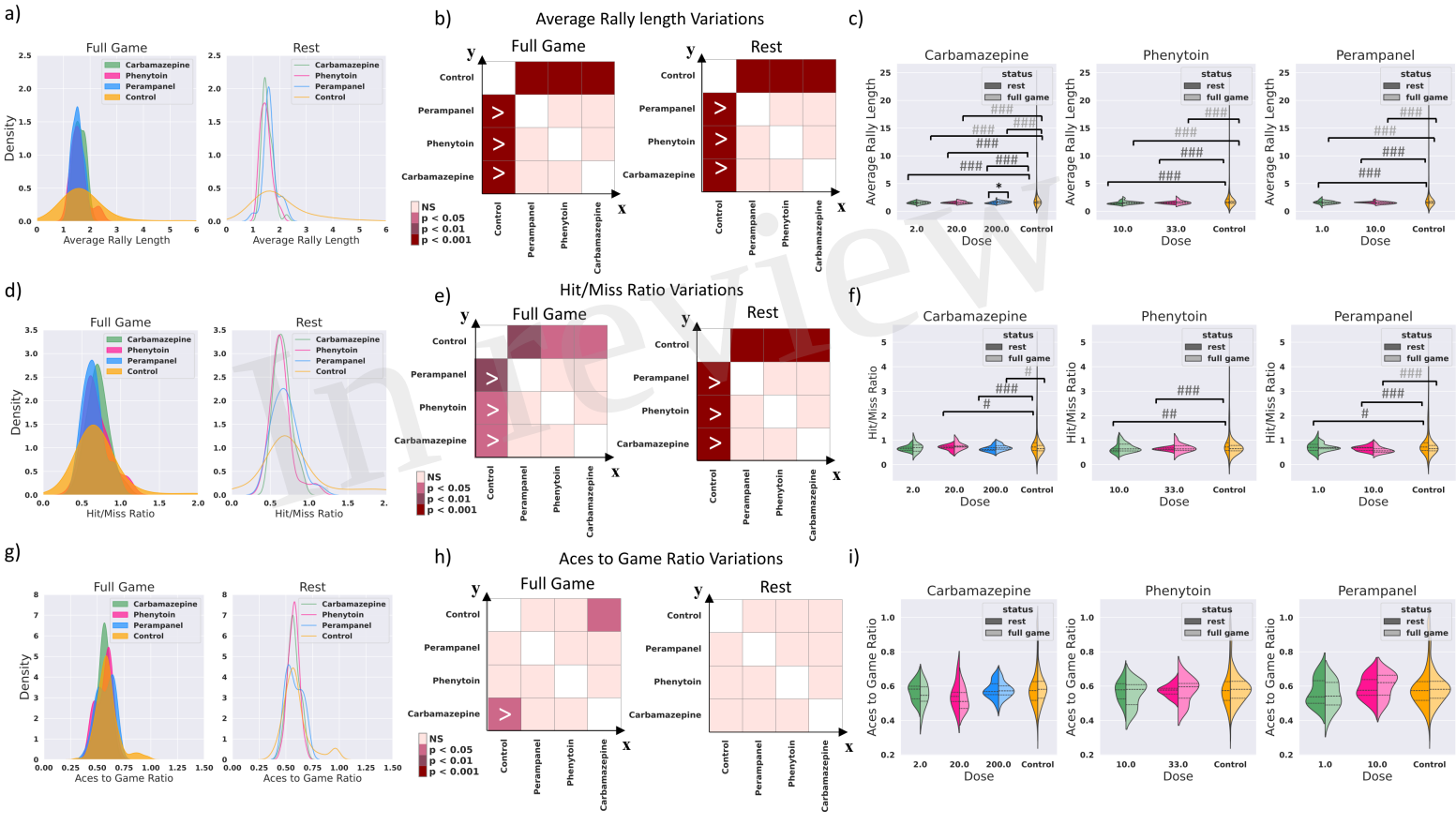
a)
Full Game
Rest
Carbamazepine
Phenytoin
Perampanel
Control
Density
Average Rally Length
b)
Average Rally length Variations
Full Game
Rest
Control
Perampanel
Phenytoin
Carbamazepine
NS
p < 0.05
p < 0.01
p < 0.001
c)
Carbamazepine
Phenytoin
Perampanel
status
rest
full game
Average Rally Length
Dose
d)
Hit/Miss Ratio
e)
Hit/Miss Ratio Variations
f)
g)
Aces to Game Ratio
h)
Aces to Game Ratio Variations
i)

Figure 6.TIF

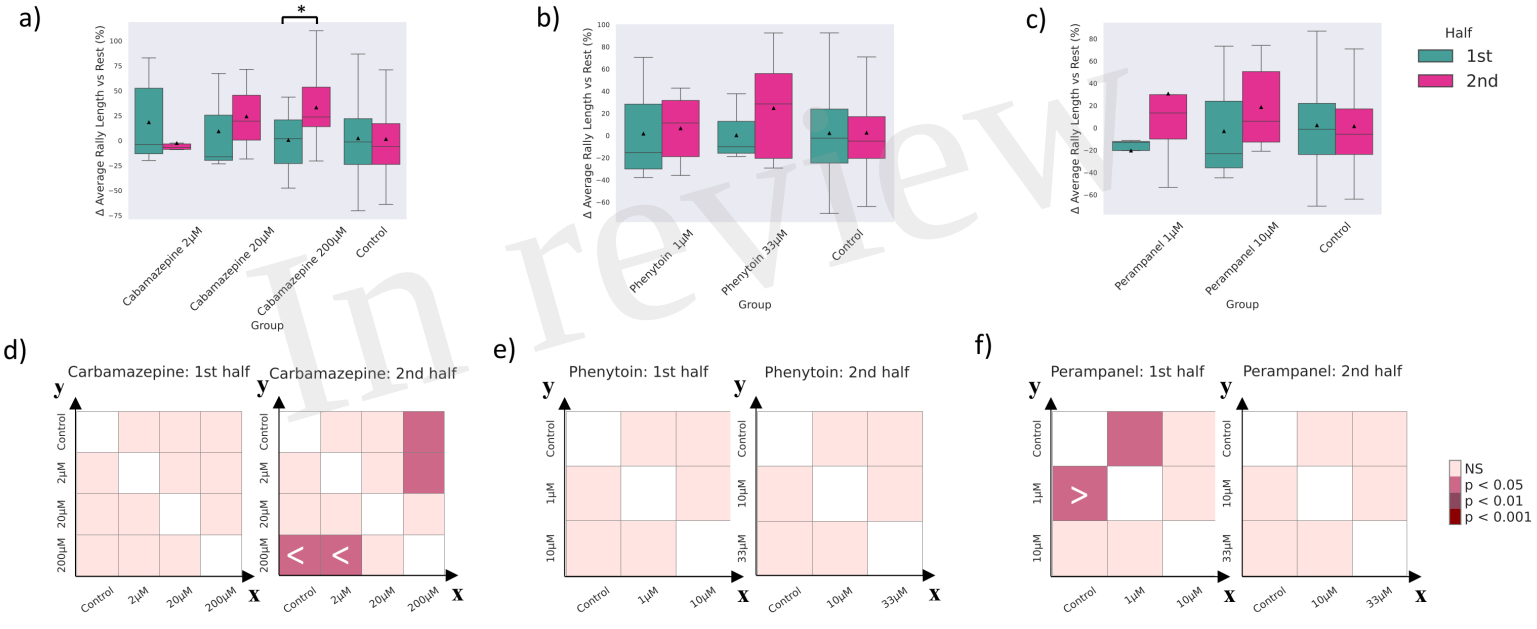

In review

Figure 7.TIF

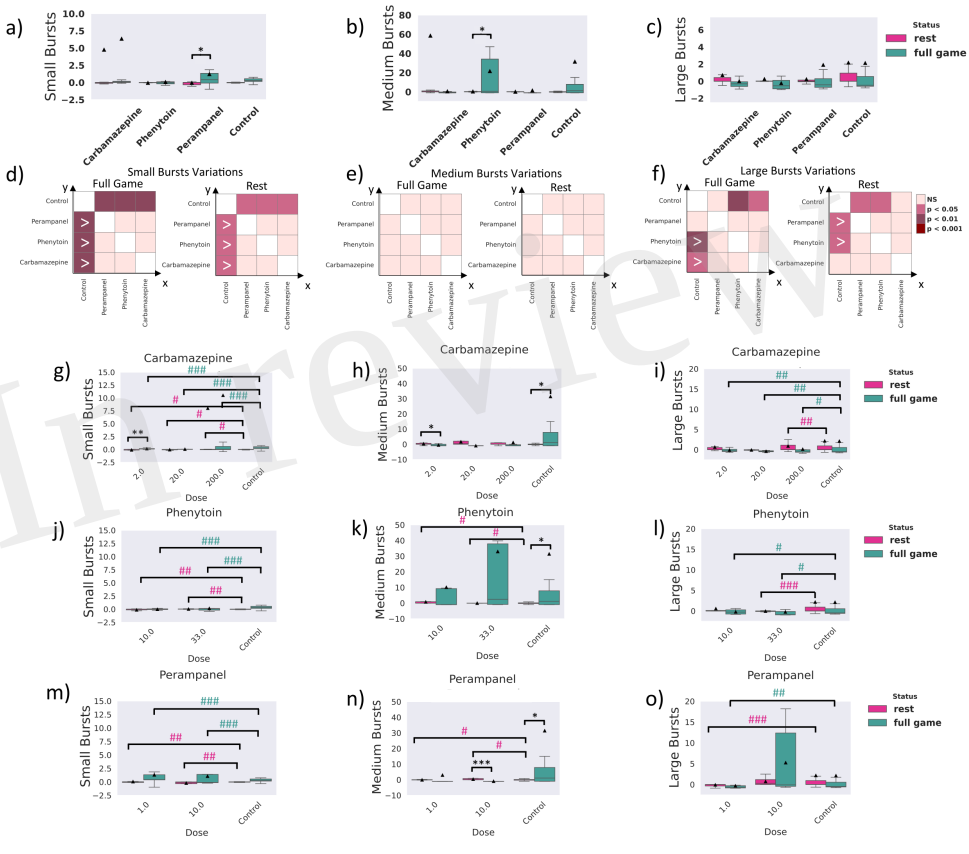

Inreview

Figure 8.TIF

a)

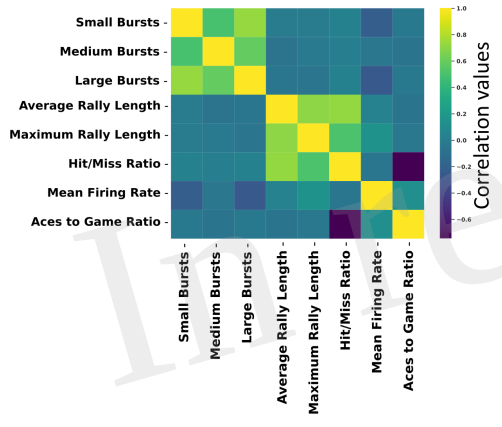

b)

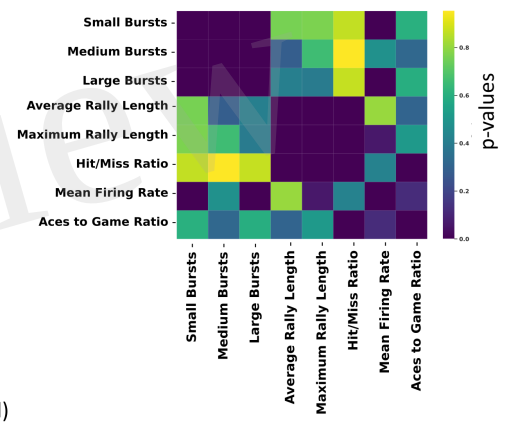

c)

Correlation values: Bursting Pattern Metrics vs. Game Performance

	Small Bursts	Medium Bursts	Large Bursts	Average Rally Length	Maximum Rally Length	Hit/Miss Ratio	Mean Firing Rate	Aces to Game Ratio
Small Bursts	1.000	0.491	0.721	-0.023	-0.023	0.013	-0.230	-0.039
Medium Bursts	0.491	1.000	0.581	-0.081	-0.033	-0.004	-0.053	-0.075
Large Bursts	0.721	0.581	1.000	-0.062	-0.064	0.012	-0.263	-0.040
Average Rally Length	-0.023	-0.081	-0.062	1.000	0.701	0.714	0.018	-0.077
Maximum Rally Length	-0.023	-0.033	-0.064	0.701	1.000	0.505	0.139	-0.049
Hit/Miss Ratio	0.013	-0.004	0.012	0.714	0.505	1.000	-0.061	-0.745
Mean Firing Rate	-0.230	-0.053	-0.263	0.018	0.139	-0.061	1.000	0.117
Aces to Game Ratio	-0.039	-0.075	-0.040	-0.077	-0.049	-0.745	0.117	1.000

d)

p-values: Bursting Pattern Metrics vs. Game Performance

	Small Bursts	Medium Bursts	Large Bursts	Average Rally Length	Maximum Rally Length	Hit/Miss Ratio	Mean Firing Rate	Aces to Game Ratio
Small Bursts	0.000	0.000	0.000	0.759	0.763	0.864	0.002	0.605
Medium Bursts	0.000	0.000	0.000	0.280	0.657	0.953	0.480	0.318
Large Bursts	0.000	0.000	0.000	0.409	0.394	0.870	0.000	0.596
Average Rally Length	0.759	0.280	0.409	0.000	0.000	0.000	0.807	0.304
Maximum Rally Length	0.763	0.657	0.394	0.000	0.000	0.000	0.063	0.512
Hit/Miss Ratio	0.864	0.953	0.870	0.000	0.000	0.000	0.419	0.000
Mean Firing Rate	0.002	0.480	0.000	0.807	0.063	0.419	0.000	0.116
Aces to Game Ratio	0.605	0.318	0.596	0.304	0.512	0.000	0.116	0.000

In review

Figure 9.TIFF

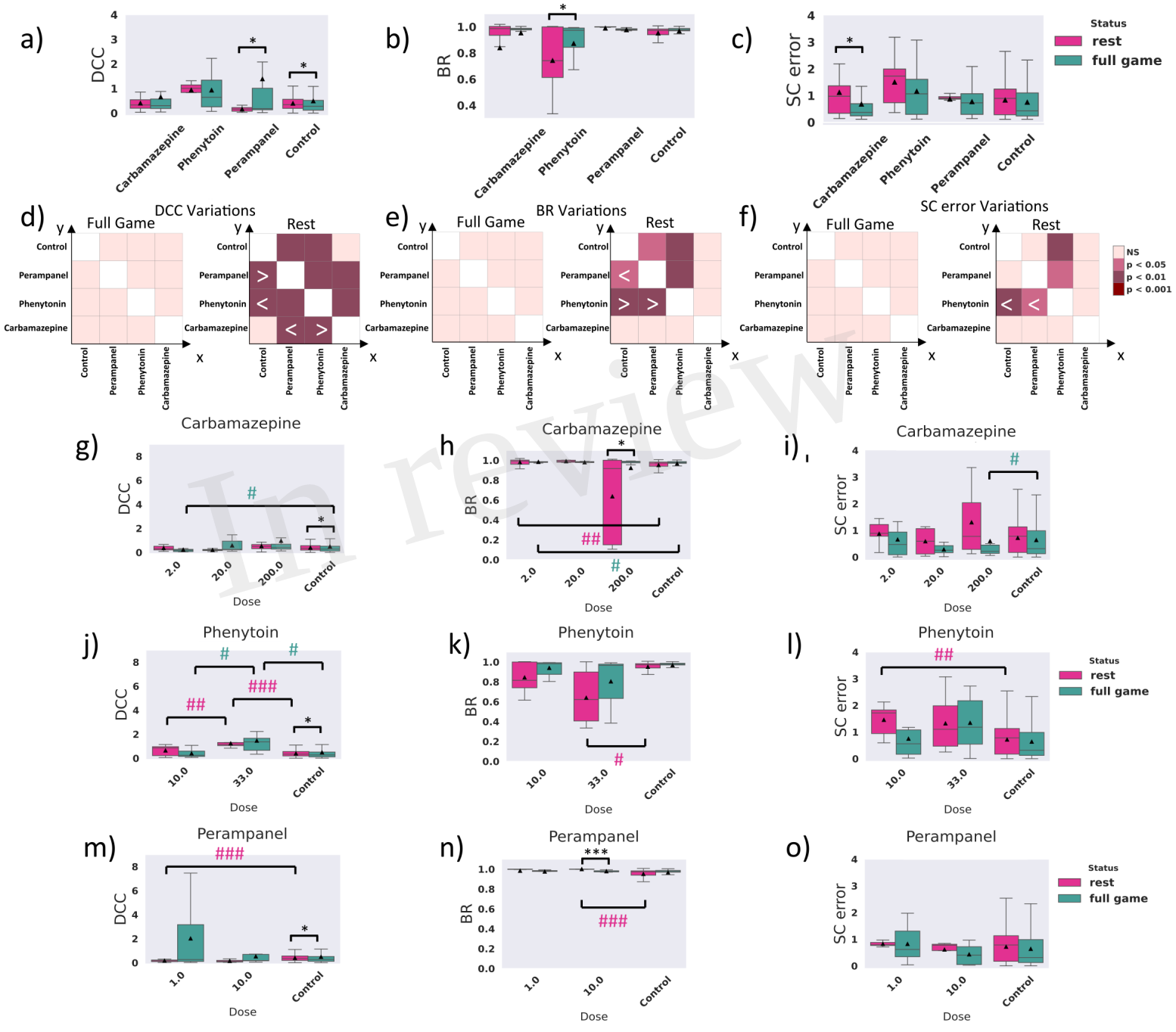

In review

Figure 10.TIF

a)

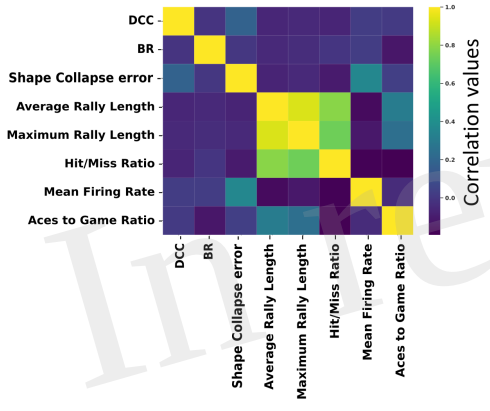

b)

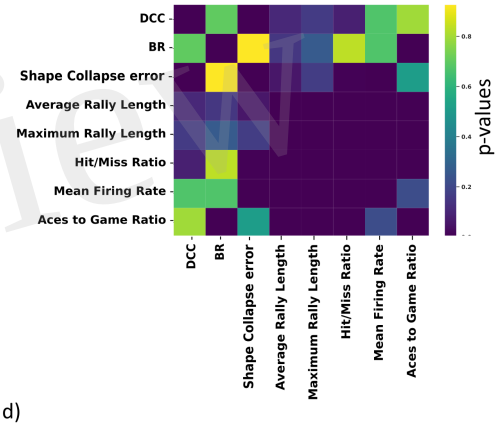

c)

Correlation values: Criticality Metrics vs. Game Performance

	DCC	BR	Shape Collapse error	Average Rally Length	Maximum Rally Length	Hit/Miss Ratio	Mean Firing Rate	Aces to Game Ratio
DCC	1.000	-0.015	0.178	-0.064	-0.055	-0.069	0.017	0.010
BR	-0.015	1.000	-0.004	-0.057	-0.044	-0.008	0.017	-0.120
Shape Collapse error	0.178	-0.004	1.000	-0.075	-0.054	-0.107	0.359	0.026
Average Rally Length	-0.064	-0.057	-0.075	1.000	0.935	0.787	-0.160	0.305
Maximum Rally Length	-0.055	-0.044	-0.054	0.935	1.000	0.739	-0.117	0.236
Hit/Miss Ratio	-0.069	-0.008	-0.107	0.787	0.739	1.000	-0.188	-0.194
Mean Firing Rate	0.017	0.017	0.359	-0.160	-0.117	-0.188	1.000	-0.049
Aces to Game Ratio	0.010	-0.120	0.026	0.305	0.236	-0.194	-0.049	1.000

d)

p-values: Criticality Metrics vs. Game Performance

	DCC	BR	Shape Collapse error	Average Rally Length	Maximum Rally Length	Hit/Miss Ratio	Mean Firing Rate	Aces to Game Ratio
DCC	0.000	0.698	0.000	0.104	0.161	0.080	0.670	0.792
BR	0.698	0.000	0.926	0.145	0.261	0.834	0.669	0.002
Shape Collapse error	0.000	0.926	0.000	0.056	0.165	0.006	0.000	0.511
Average Rally Length	0.104	0.145	0.056	0.000	0.000	0.000	0.000	0.000
Maximum Rally Length	0.161	0.261	0.165	0.000	0.000	0.000	0.003	0.000
Hit/Miss Ratio	0.080	0.834	0.006	0.000	0.000	0.000	0.000	0.000
Mean Firing Rate	0.670	0.669	0.000	0.000	0.003	0.000	0.000	0.215
Aces to Game Ratio	0.792	0.002	0.511	0.000	0.000	0.000	0.215	0.000

Inreview

Figure 11.TIF

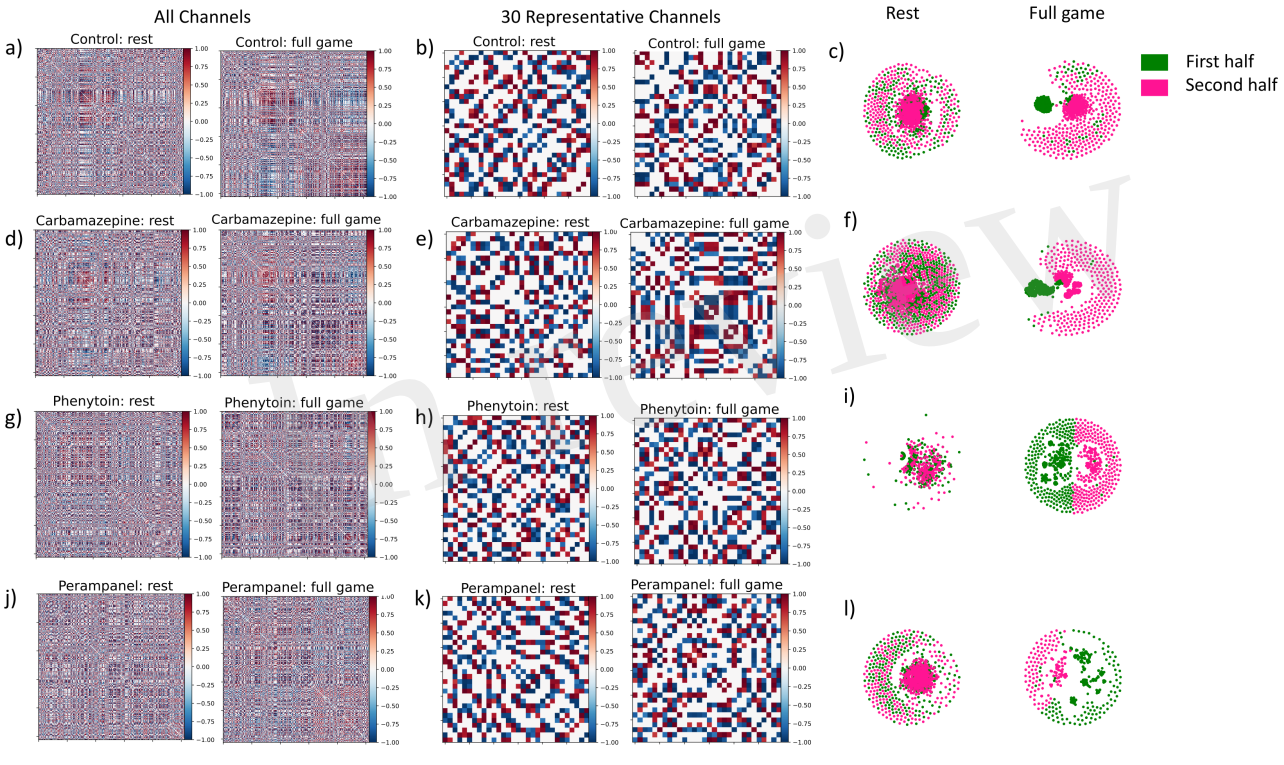

Figure 12.TIF

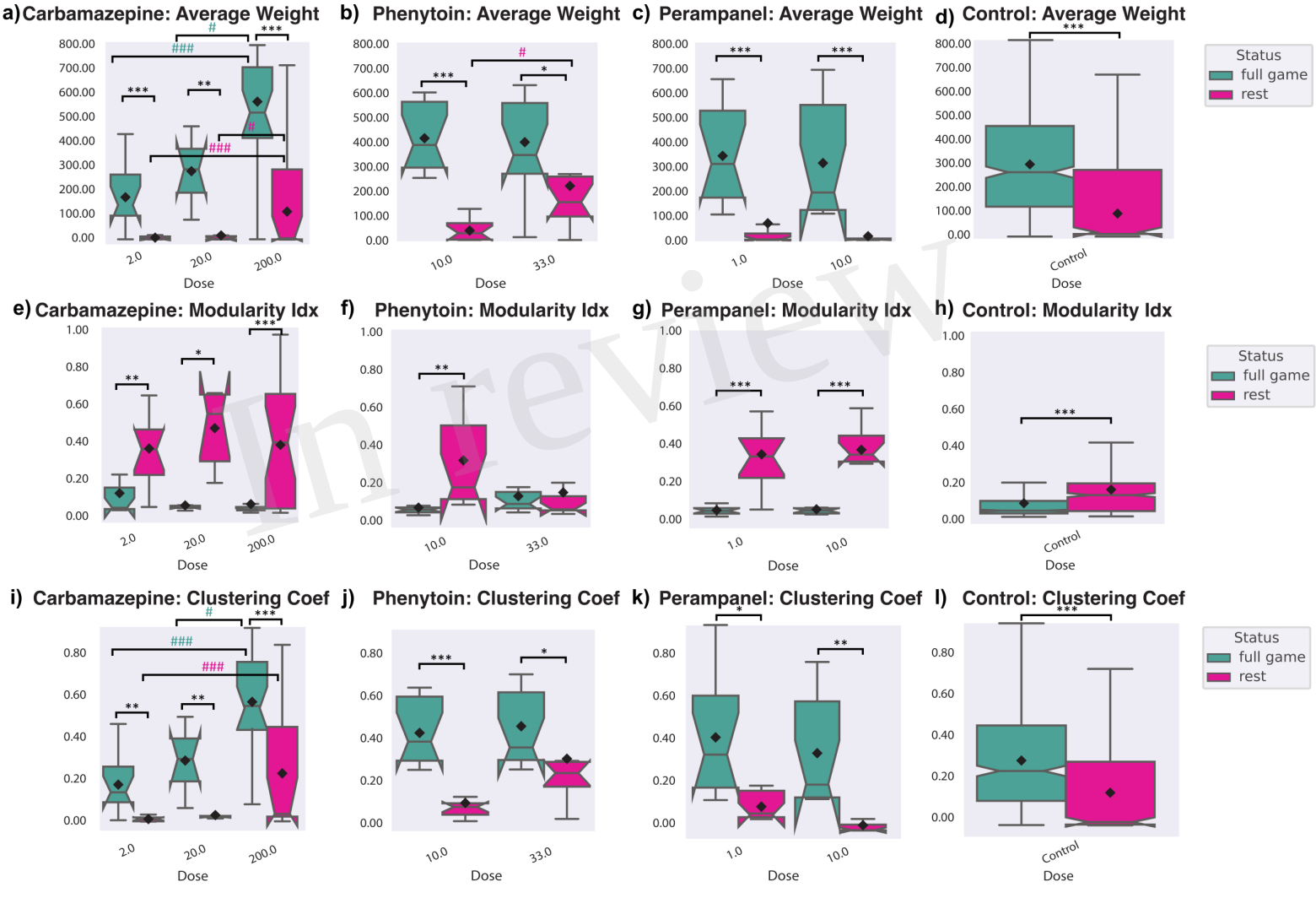

In review

Figure 13.TIF

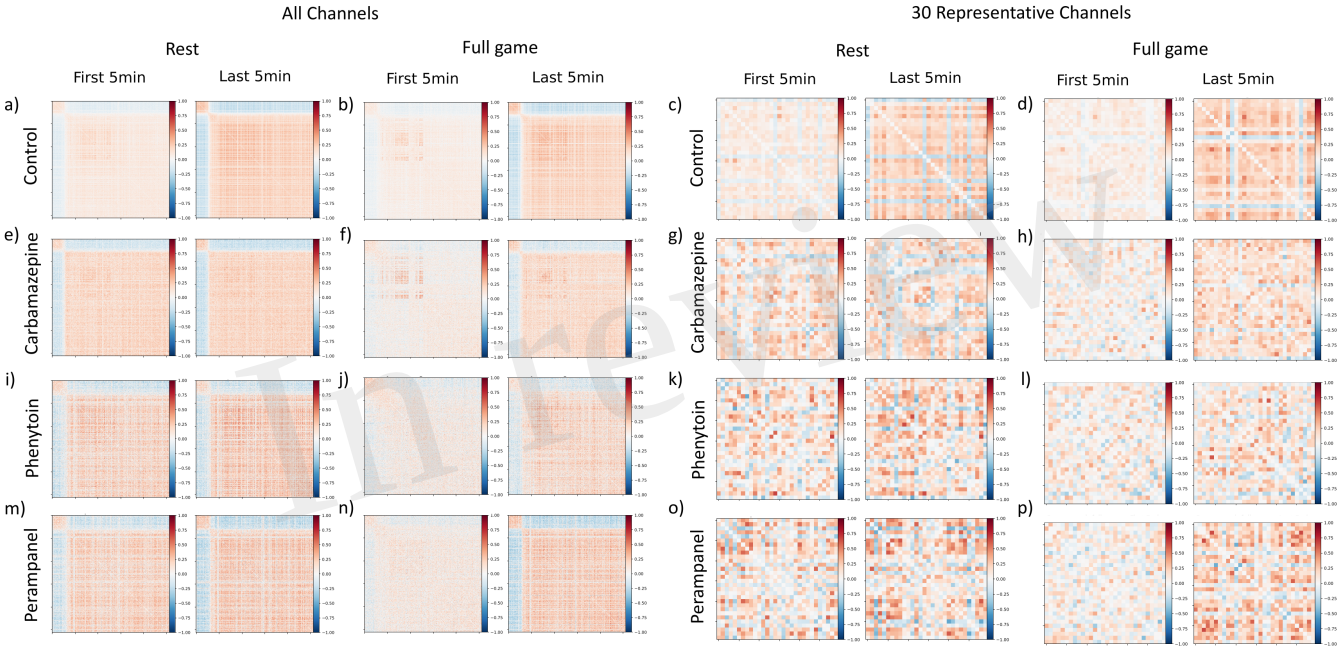

Figure 14.TIF

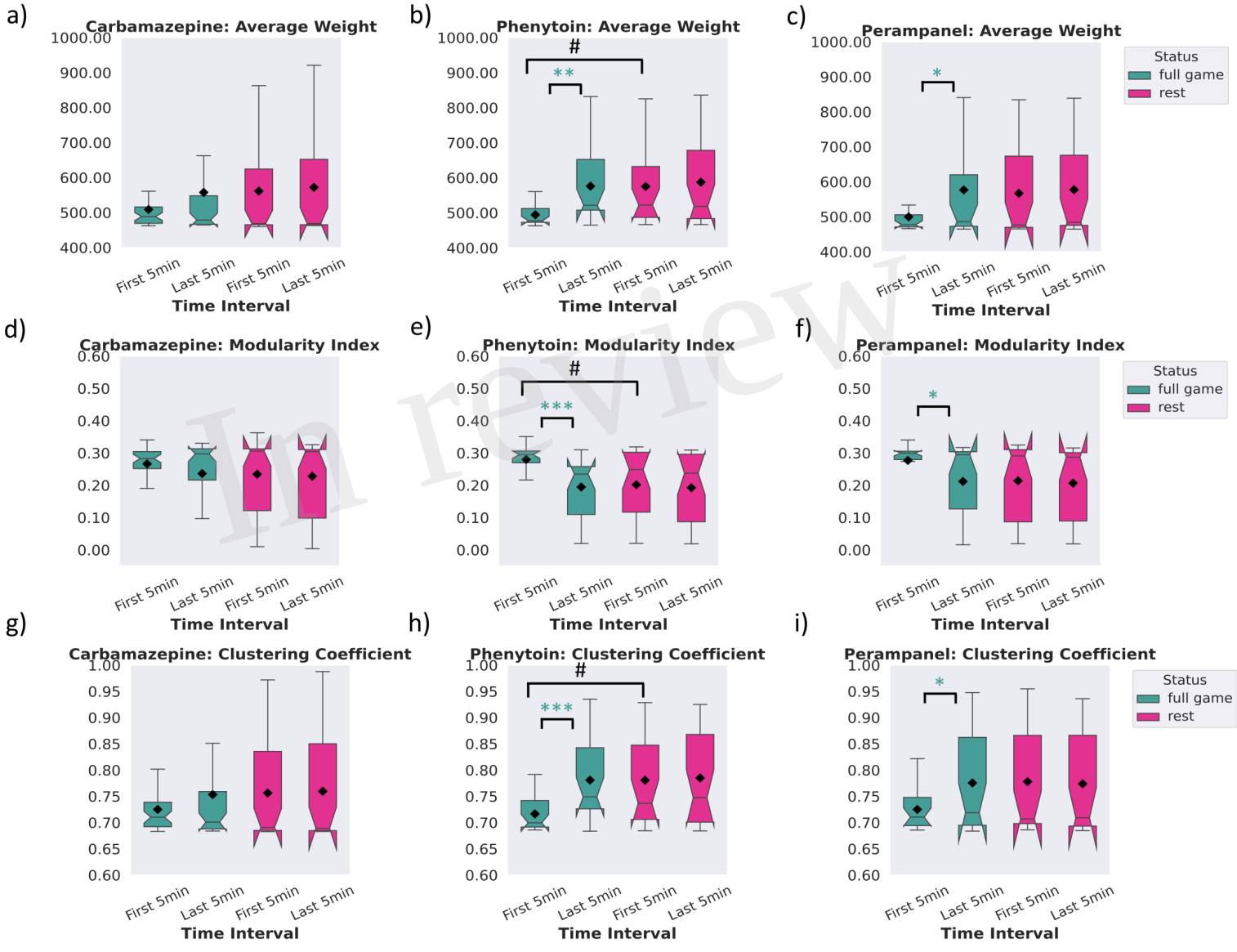

In review

Figure 15.TIF